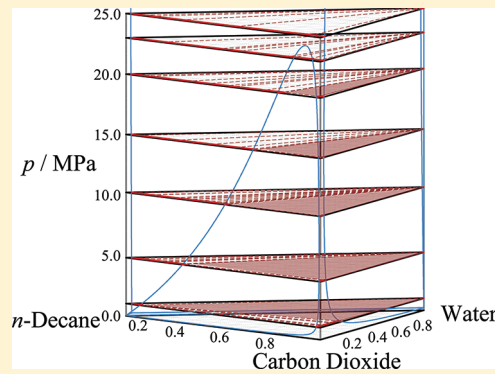


# Experimental and Molecular Modeling Study of the Three-Phase Behavior of (*n*-Decane + Carbon Dioxide + Water) at Reservoir Conditions

Esther Forte, Amparo Galindo, and J. P. Martin Trusler\*

Department of Chemical Engineering, Imperial College London, London SW7 2AZ, U. K.

**ABSTRACT:** Knowledge of the phase behavior of mixtures of oil with carbon dioxide and water is essential for reservoir engineering, especially in the processes of enhanced oil recovery and geological storage of carbon dioxide. However, for a comprehensive understanding, the study of simpler systems needs to be completed. In this work the system (*n*-decane + carbon dioxide + water) was studied as a model (oil + carbon dioxide + water) mixture. To accomplish our aim, a new analytical apparatus to measure phase equilibria at high pressure was designed with maximum operating temperature and pressure of 423 K and 45 MPa, respectively. The equipment relies on recirculation of two coexisting phases using a two-channel magnetically operated micropump designed during this work, with sampling and online compositional analysis by gas chromatography. The apparatus has been validated by comparison with published isothermal vapor–liquid equilibrium data for the binary system (*n*-decane + carbon dioxide). New experimental data have been measured for the system (*n*-decane + carbon dioxide + water) under conditions of three-phase equilibria. Data for the three coexisting phases have been obtained on five isotherms at temperatures from 323 to 413 K and at pressures up to the point at which two of the phases become critical. The experimental work is complemented here with a theoretical effort in which we developed models for these molecules within the framework of the statistical associating fluid theory for potentials of variable range (SAFT-VR). The phase behavior of the three binary subsystems was calculated using this theory, and where applicable, a modification of the Hudson and McCoubrey combining rules was used to treat the systems predictively. The experimental data obtained for the ternary mixture are compared to the predictions of the theory. Furthermore, a detailed analysis of the ternary mixture is carried out based on comparison with available data for the constituent binary subsystems. In this way, we analyzed the observed effects on the solubility when the third component was added.



## INTRODUCTION

Carbon dioxide has been used as an injection gas for enhanced oil recovery (EOR) purposes since the early 1970s. The project at the SACROC unit (Kelly-Snyder field, Scurry County, West Texas) initiated in 1972 was one of the first; pressures below 17 MPa<sup>1,2</sup> were used in a water-alternating-gas project. Since then, it has become an attractive alternative in cases in which a relatively low-cost source of CO<sub>2</sub> is available. In most of the cases naturally occurring CO<sub>2</sub> is used.<sup>3</sup> But because of their known geologic seal, oil reservoirs are also a favorable option for sequestering anthropogenic CO<sub>2</sub>.<sup>4</sup> In an ideal scenario, CO<sub>2</sub> that has been captured from a power plant would be used for EOR first and then stored in the reservoir afterward. The first project involving both CO<sub>2</sub>-EOR and also the storage of CO<sub>2</sub> of anthropogenic origin commenced at the Weyburn field<sup>5–7</sup> (Saskatchewan, Canada) in 2000.

The miscibility of carbon dioxide with oil plays an essential role in both CO<sub>2</sub>-EOR and CO<sub>2</sub> storage processes. In EOR, the objective of the CO<sub>2</sub> injection is to mobilize the residual oil by dissolution; this oil is in the form of drops that remained trapped in the pore structure of the reservoir rock after secondary oil recovery. The interfacial tension between oil and water also plays

an important role in such trapping mechanism. The CO<sub>2</sub> injected is likely to form two phases with the existing oil at reservoir conditions, and a third phase will typically coexist due to the presence of water. Water may also be added at this stage to improve the efficiency of the sweeping process in alternating injection steps with the CO<sub>2</sub>. The CO<sub>2</sub>-rich phase contains some light hydrocarbons and flows easily; a considerable portion of the CO<sub>2</sub> will also dissolve in the oil-rich phase. In general, dissolution of the CO<sub>2</sub> reduces the interfacial tension of the oil against water,<sup>8</sup> promoting coalescence of the drops; the viscosity of the oil is reduced,<sup>9</sup> and its mobility is increased. Ideally, however, total miscibility is pursued, and the minimum miscibility pressure (MMP) obtained from experiments at laboratory scale is an important parameter in optimizing the efficiency of the extraction. Characteristic reservoir conditions are commonly understood to be on the order of  $T = 330\text{--}470$  K with pressure conditions of 10–200 MPa. The essential input for CO<sub>2</sub>-EOR processes from phase equilibria measurements is however

**Received:** July 16, 2011

**Revised:** October 24, 2011

**Published:** October 26, 2011

limited to pressures below the bubble curve including the critical locus along which miscibility of CO<sub>2</sub> with hydrocarbons in the presence of water is achieved at reservoir temperatures. Regarding the sequestration of CO<sub>2</sub>, although structural and capillary trapping are known to be the primary forces, dissolution of the CO<sub>2</sub> is one of the long-term mechanisms for sequestering CO<sub>2</sub> in the reservoir.

Acquiring a comprehensive understanding of the behavior of carbon dioxide mixtures under reservoir conditions is essential for optimizing usage and developing sequestration schemes. Because of the complexity of oil mixtures, a necessary step is the completion of a database comprising simpler systems that may represent certain characteristics of the real ones. In so doing it is necessary to account for the presence of water in the reservoir. In spite of the attention that binary combinations of alkanes, carbon dioxide, and water have received, experimental data concerning ternary mixtures are sparse. Among the published data for ternaries of the type (*n*-alkanes + carbon dioxide + water), mixtures of (methane + carbon dioxide + water) have been the most widely studied, not only regarding fluid-phase equilibria<sup>10–13</sup> but also fluid–hydrate equilibria.<sup>14–16</sup> Other studies have concerned the systems (ethane + carbon dioxide + water),<sup>11</sup> (propane + carbon dioxide + water),<sup>17</sup> and (butane + carbon dioxide + water)<sup>17</sup> at low temperatures and pressures. Most of these studies for fluid-phase equilibrium in ternary mixtures focused on vapor–liquid equilibrium (VLE), and only one phase composition was typically measured. Only in the study of Song and Kobayashi<sup>13</sup> were measurements made along the three-phase equilibrium locus, although again only one phase was analyzed. Regarding heavier hydrocarbons, there is one experimental study of (*n*-hexadecane + carbon dioxide + water);<sup>18</sup> mainly VLE was measured at pressures between 10 and 30 MPa and temperatures between 473.15 and 573.15 K, although one experimental point was reported in the three-phase equilibrium region at 473.15 K and 20 MPa. In this study it was reported that although typically a sampling technique based on capillaries and online chromatographic analysis was used, for *n*-hexadecane a method based on cold traps was required to avoid condensation during transport to the chromatograph.<sup>18</sup>

In this work, the system (*n*-decane + carbon dioxide + water) was studied as a model (oil + carbon dioxide + water) mixture. To our knowledge, this system has been the subject of only one previous experimental study<sup>19</sup> involving a rather complex technique based on PVT measurements with a fiberoptic scope to locate interfaces. The composition of the equilibrium phases was not directly measured but rather calculated on the basis of the overall density at the conditions of study and the use of a thermodynamic model. The data reported however disagree with the nature of the interactions between the components of the mixture. The immiscibility of the subsystems (water + CO<sub>2</sub>) and (water + *n*-decane) at the conditions of the experiments indicate that a three phase region occupies an important part of the diagram. However, three-phase equilibria were not observed at all in the mentioned study, nor predicted, and high compositions of water were reported for the single mixed liquid phase. Consequently, the experimental results reported by Okafor<sup>19</sup> do not appear to be meaningful.

The extreme phase behavior and consequent low solubilities of alkanes and CO<sub>2</sub> in water for large temperature ranges up to the critical temperature of water (647 K) makes these aqueous systems extremely complex to measure. Both (carbon dioxide + water) and (*n*-decane + water) exhibit type III phase behavior in

the classification of Scott and van Konynenburg;<sup>20,21</sup> this is characteristic of very immiscible systems with a wide region of liquid–liquid equilibria that extends to high temperatures. The complexity is apparent from the scatter found in the literature data for (carbon dioxide + water) (see reviews<sup>22,23</sup>). The phase behavior is even more extreme in the case of (alkane + water) systems, where there is also a significantly smaller amount of data for the binary (*n*-decane + water).<sup>24</sup> A special experimental difficulty is achieving reliable sampling and subsequent analysis; precautions are needed with *n*-decane to avoid condensation, and also with water to avoid adsorption problems during transport to the gas chromatograph. Experimental measurements of these aqueous systems published in the literature are in many studies focused on one of the phases using a synthetic-type apparatus, thus avoiding sampling. The different volatility of the components of interest in this study also affects the reliability of the sampling technique. A new experimental apparatus has therefore been developed for this work incorporating micro sampling and online chromatographic analysis. Recirculation of two phases is performed by a new magnetically coupled reciprocating pump, designed and built during this work.

From a modeling perspective, it is common practice in reservoir engineering to use cubic equations of state such as the Peng–Robinson (PR)<sup>25</sup> or Soave–Redlich–Kwong (SRK)<sup>26</sup> equations. These equations are based on the same model as that of van der Waals.<sup>27</sup> The latter constitutes a sound basis for describing spherical molecules interacting through long-range dispersive interactions; unfortunately, such models may not be appropriate for systems which exhibit hydrogen bonding or for highly asymmetric molecules. A number of equations of state which specifically include a treatment of directional interactions (association) at the molecular level have been used to study hydrogen bonding fluids. One of these treatments is the cubic plus association (CPA) EOS,<sup>28</sup> which combines the SRK EOS with the thermodynamic perturbation theory of Wertheim.<sup>29–32</sup> This perturbation theory was first incorporated in the foundations of the statistical associating fluid theory (SAFT)<sup>33,34</sup> which explicitly takes into account not only directional interactions<sup>29–32</sup> but also the nonsphericity or chainlike nature of many molecules.<sup>35,36</sup> There are numerous versions of the SAFT treatment, such as the SAFT-VR<sup>37,38</sup> (variable range) equation used in this work, soft-SAFT,<sup>39</sup> and PC-SAFT<sup>40,41</sup> (see reviews<sup>42–46</sup>).

Mixtures of alkanes and/or carbon dioxide with water have received attention in the literature not only because of their practical interest but also because of the theoretical challenges presented in attempting to model such systems accurately. Both types of systems are known to form highly nonideal mixtures due to the strong association of water. In spite of the difficulties, the global phase behavior of (alkane + water) has been successfully modeled using associating theories.<sup>47–55</sup> One of the latest techniques used to model the phase behavior of (alkane + water) systems is the SAFT- $\gamma$  approach;<sup>56</sup> this is a recast version of the SAFT-VR equation of state with a group contribution formalism that enables successful predictions for these systems based on transferable interaction parameters. All these procedures can provide a reasonably good level of agreement with experiment, but the accurate prediction of both the aqueous-rich and the alkane-rich phases with a single interaction parameter is not easily achieved. Recently, new combining rules have been proposed on the basis of those of Hudson and McCoubrey,<sup>57</sup> which predict different values of the common  $k_{ij}$  binary interaction parameter of each phase depending on differences in the

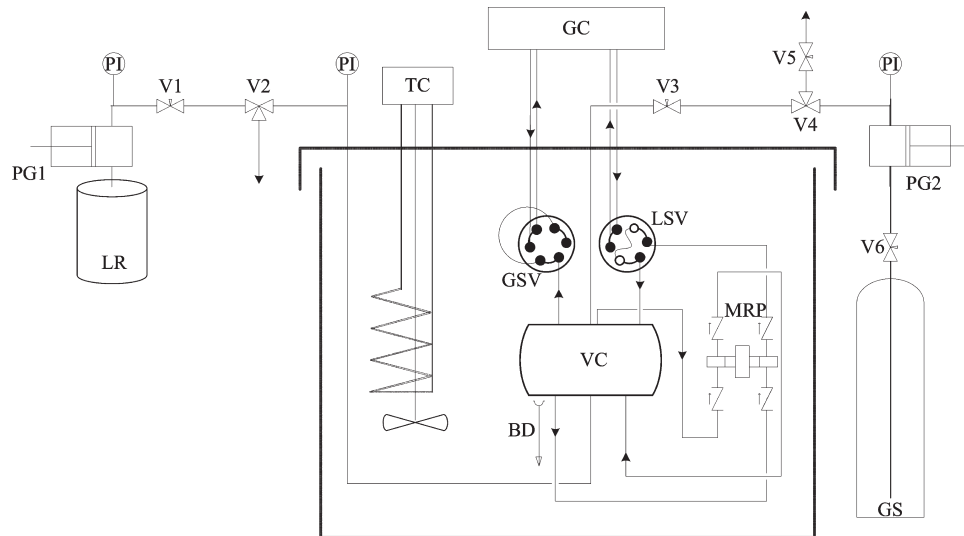


**Figure 1.** Schematic diagram of the static-analytical apparatus. The following components are depicted: view-cell, VC; magnetic recirculation pump, MRP; liquid sampling valve, LSV; gas sampling valve, GSV; gas-chromatograph, GC; temperature controller, TC; pressure transducers, PI; pressure generators, PG1 and PG2; bursting-disk, BD; liquid reservoir, LR; and gas cylinder, GS.

dielectric constant of the phases and dipole moment of the molecules; these differences are relevant in mixtures including strongly polar components such as water.<sup>58</sup> Another interesting feature of these systems not easily reproduced by models adjusted to describe the global behavior of the mixtures is the solubility minima found experimentally<sup>59,60</sup> for hydrocarbons in water. Studies with different SAFT equations have shown good agreement when tuned in the region of interest.<sup>61,62</sup> Mixtures of (carbon dioxide + water) have not lacked attention either. CO<sub>2</sub> has no net dipole moment, and it is typically modeled as a non-self-associating molecule. However, it is strongly quadrupolar and in water partially dissociates to form carbonic acid; this has led a number of authors to model the interactions between the two components as associating. A cross-associating model of this type has been found useful to reproduce with the CPA EOS the change in curvature that characterizes the solubility curve of water in the CO<sub>2</sub>-rich phase;<sup>63,64</sup> this model has also been applied recently to multicomponent mixtures, such as (methane + carbon dioxide + water).<sup>65</sup> Similar cross-associating interactions for (carbon dioxide + water) were suggested by Valtz et al. who used the SAFT-VR equation,<sup>66</sup> this time considering the possibility of CO<sub>2</sub> as a self-associating compound; however a value close to zero was found for the resulting bonding energy leading to the conclusion that the additional interaction is not needed. Later studies of the same system with the SAFT-VR equation have resulted in similar findings: the properties of (carbon dioxide + water) can be predicted accurately without incorporating association between the two species.<sup>67–69</sup> More rigorous models for CO<sub>2</sub> can additionally be considered by incorporating the contribution of the molecular quadrupole into the equation of state.<sup>70,71</sup> Regarding the study of ternaries and, in general, multicomponent mixtures, a question arises. Because all equations of state are based on pair-potential formalisms there is the question as to whether or not binary parameters can always predict the phase behavior of multi-component mixtures; the answer may be that this is not always successful. The underlying difficulties emphasize the need for experimental data on these systems.

In the remainder of this paper, we describe the apparatus in detail and we present validation measurements and a comparison

with published vapor–liquid equilibrium data for the system (*n*-decane + carbon dioxide). We present a large body of new liquid–liquid equilibrium (LLE) and vapor–liquid–liquid equilibrium (VLLE) data for the system (*n*-decane + carbon dioxide + water). We compare our experimental findings with the predictions of SAFT-VR.<sup>37,38</sup> We use this method as it has already been shown in a number of studies<sup>67–69,72–74</sup> to provide an accurate description of the phase behavior of mixtures consisting of alkanes, CO<sub>2</sub>, and water, for wide ranges of thermodynamic conditions. Finally, where possible, further comparisons with data for the binary subsystems are also presented.

## ■ EXPERIMENTAL SECTION

**Apparatus.** A new static-analytical apparatus was designed for the purpose of analyzing phase behavior at conditions of temperatures and pressures ranging from 253 to 423 K and from 0.5 to 45 MPa, respectively. The main components, seen in Figure 1, are a high-pressure view-cell, a magnetically coupled reciprocating pump (both fabricated in-house), electronically actuated sampling valves (Cheminert, model C2-2206EH3Y, and Valco, model DCI4UWT1Y, VICI AG International), and a gas chromatograph (Shimadzu, model GC-2014, Shimadzu Scientific Instruments, Inc.). A manual syringe pump (Sitec model 750.1100, SITEC-Sieber Engineering AG) was used for loading liquid components; an automatic syringe pump (Teledyne Isco, model 100DM, Teledyne Technologies Inc.) was used for loading carbon dioxide. The syringe of this pump was maintained at a temperature of 283 K by means of a cooling jacket through which water was circulated by a chiller unit (Huber minichiller-NR, Huber Kältemaschinenbau GmbH). The remaining circuits shown in Figure 1 were used for purposes of venting, flushing, and draining the system. The vessel, the reciprocating pump, and the sampling valves were located inside a temperature-controlled oil bath.

**Main Body.** The main component in the setup was an equilibrium cell, described previously,<sup>75</sup> made from type 17-4PH martensitic stainless steel. It had a nominal internal volume of 35 cm<sup>3</sup>. The cell held two diametrically opposite sapphire

windows that enabled visual observation of the interior. This not only made the measurements easier to perform, but also was essential for observing the formation of phases, especially with more than two phases. The windows were also useful in this work for observing critical opalescence. O-rings made of hydrogenated nitrile (elast-O-Lion 101, James Walker and Co.) were used to seal the windows to the vessel, and these proved to be robust in contact with CO<sub>2</sub>. Threaded rings retained the sapphire windows while direct contact was avoided by annular gaskets of PTFE.

Apart from common connections for 6.4 mm diameter high-pressure tubing, the cell was also equipped with plugs<sup>75</sup> that permitted a zero-dead volume connection of capillary tubing, and these were used for the sampling lines in this work. Hydrogenated nitrile o-rings were used here also. One plug, at the top of the cell, accommodated 1.6 mm o.d., 0.1 mm i.d., capillary tube for the withdrawal of the lightest phase. The three remaining plugs were used to accommodate 1.6 mm o.d., 1 mm i.d., stainless steel tubing linked to the recirculation pump: one at the bottom for the withdrawal of the heaviest phase and the other two for returning fluid back to the cell. The fact that these plugs were longitudinally off-center made it possible to withdraw a third middle phase. This was achieved by a tilting mechanism operated by a pneumatic cylinder linked to the cell by a push rod. This facility was also used to promote mass transfer inside the cell by rocking the vessel with a range of  $\pm 40^\circ$ .

The remaining high-pressure connections, four in total, were used with reducers to fit 1.6 mm o.d. tubes for the liquid (0.25 mm i.d.) and gas inlet (0.25 mm i.d.), the rupture-disk safety head (HiP model 60-61HM4, High Pressure Equipment Company), and the inlet for the vapor recirculation loop (1 mm i.d.). This and the previous connections are shown in Figure 1. The pressure transducer (Digiquartz model 410KR-HT-101, Paroscientific Inc., full scale range 69 MPa) was connected to the liquid inlet line. This transducer was regulated at a fixed temperature of 313.15 K and was calibrated against a pressure balance (Desgranges et Huot, model 26000) fitted with a piston-cylinder unit having a full-scale range of 50 MPa and expanded relative uncertainty of 0.01%. The calibration was done in a range of pressures from 0.1 to 50 MPa, and the final uncertainty of the pressure measurements was estimated to be 10 kPa. In order to account for any sensor drift over time, the pressure readings of the transducer were periodically compared at ambient pressure against a digital barometer located in the same laboratory, and small additive corrections were made to account for the observed differences.

The cell was placed inside a purpose-built temperature regulated stainless steel bath. It contained two double-glazed windows, at the front and back, which were aligned with the sapphire windows of the cell. Back illumination (with an LED light source fitted with a diffuser) and a camera in front mounted on an optical rail facilitated the observation of the inside of the cell. The space in between the double glazing was filled with argon to avoid condensation of water vapor from the air at low temperatures. The bath was fitted with a commercial stirrer and temperature-controller unit (Grant model GR150, Grant Instruments Ltd.). Silicon oil (Dow Corning Corporation, type 200-10) was used as the thermal fluid inside the bath, limiting the maximum operating temperature to about 433 K. The temperature was measured by means of a platinum resistance thermometer (PRT) located in the bath close to the equilibrium cell. The PRT was calibrated on ITS-90 at the temperature of the triple-point of water and by comparison with a standard platinum resistance thermometer in

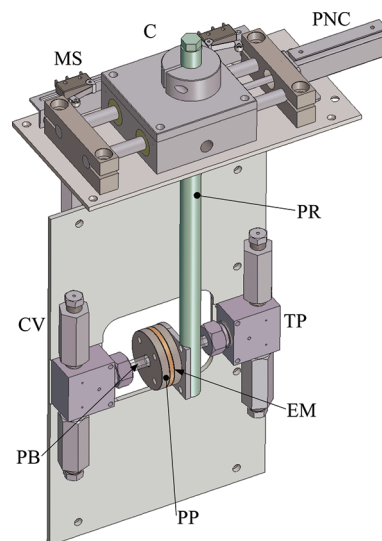


**Figure 2.** Three-dimensional view of the magnetic recirculation pump. The following components are depicted: pump body (including internal piston), PB; magnet assembly including the external magnet, EM, and the pole pieces, PP; check-valves, CV; “tee” unions, TP; push-rod, PR, and carrier for the magnet, C; microswitches, MS; pneumatic-cylinder, PNC.

a constant temperature bath at temperatures up to 473 K. The uncertainty of the PRT was 0.02 K, but fluctuations of the bath temperature could be as much as  $\pm 0.05$  K. Consequently, the overall uncertainty of the cell temperature was taken to be 0.05 K. A coil connected to an additional external circulating bath (Huber model CC1, Huber Kältemaschinenbau GmbH) was used to provide refrigeration when working at temperatures near or below ambient. A motorized elevator was used to raise and lower the oil bath.

**Reciprocating Pump and Sampling System.** During this work a magnetically coupled reciprocating pump (see Figure 2) was designed and built, which was able to work at conditions of high pressure and temperature. It was based on a previous design<sup>76</sup> implemented on a smaller scale and with two separate flow channels. The latter characteristic was used to recirculate two of the equilibrium phases simultaneously; i.e., liquid was pumped through one channel, while vapor was sucked through the other. The circulation of both liquid and vapor was advantageous to promote mass transfer between the phases. The vapor was bubbled from the bottom of the cell, passing through all the coexisting liquid phases. The liquid dropped from the top of the cell through the vapor and, where present, the second liquid phase.

The recirculated liquid was used for sampling. The position of the pump was such that the liquid passing through the sampling valve was subjected to a slightly elevated pressure; i.e., the sampling valve was located downstream of the pump. The vapor phase was sampled directly from the equilibrium vessel using a small-bore capillary of minimum internal volume, with the dimensions previously given, independent of the recirculation loop. The liquid valve was a 4-port valve with an internal sampling loop of volume 1 mm<sup>3</sup>. A 6-port valve fitted with a 5 mm<sup>3</sup> external sample loop was used for the vapor. The valves were electronically actuated and were kept at the same temperature as the cell to avoid condensation.

The pump, shown in Figure 2, was magnetically coupled. To ensure sufficient magnetic coupling between the external permanent

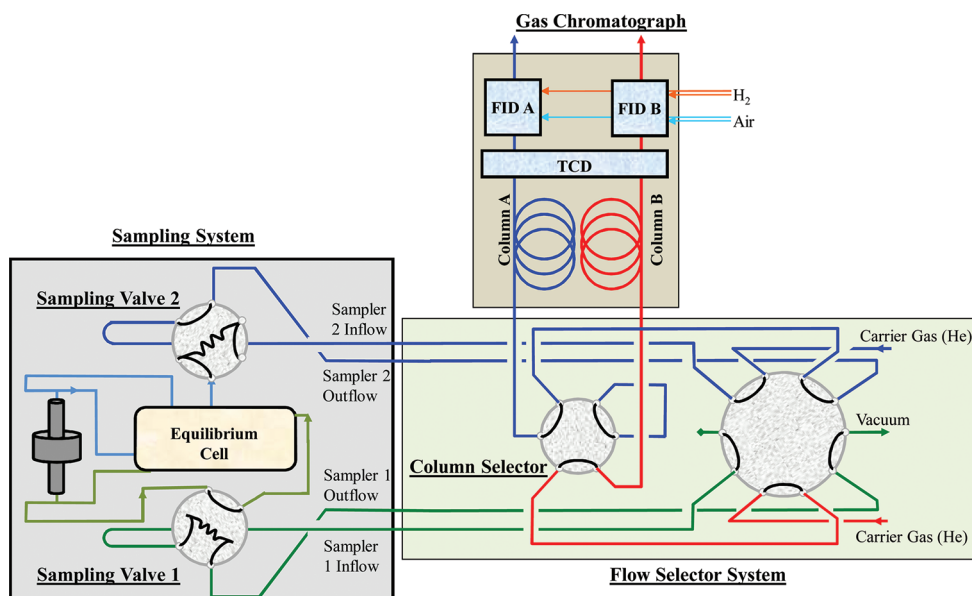


Figure 3. Schematic diagram of the connections between the gas chromatograph and the sampling system.

magnet and the internal magnetic piston, the magnetic circuit design was optimized by means of finite element analysis. Where possible, the pump was fabricated from parts that were commercially available. The body of the pump consisted of a type AISI 316 L stainless steel nipple of 6.4 mm external diameter and length 100 mm that was gun drilled and honed to an i.d. of 3.00 mm. The internal piston, of 15 mm length and 2.95 mm diameter, was fabricated from a magnetic stainless steel, AISI type 431, chosen for its corrosion-resistant properties. Elastomeric seals, which may easily swell in contact with CO<sub>2</sub>, were avoided. Since vapor sampling was not made in the recirculation loop, leakage from the liquid side to the gas side was not a problem. In the liquid loop, the sampling valve provided sufficient back pressure as to prevent gas leakage into the liquid stream. The external magnet comprised an annular ring of neodymium N45SH (outside diameter 35.6 mm, inside diameter 8.60 mm, length 3 mm) placed between two mild-steel pole pieces (outside diameter 35.6 mm, inside diameter 7.00 mm, length 5 mm).

Each side of the nipple was attached to a reducing “tee” union (Sitec custom-made, SITEC-Sieber Engineering AG) to connect to 1.6 mm o.d. high-pressure tubing. Four check valves (Sitec model 620.4311 and 620.4312, SITEC-Sieber Engineering AG) ensured unidirectional flow in each channel. To enhance the efficiency of the pump, we reduced the dead volume within the check valves with a cylindrical insert of our own design and replaced the poppet with a type 316 stainless steel ball of 3.0 mm diameter. We also dispensed with the internal spring, to reduce the cracking pressure, and relied instead upon gravity to close the check valves.

To drive the external magnet, a double-acting pneumatic cylinder was used. This was operated in conjunction with a double solenoid valve and flow and pressure regulators. Micro-switches were used at the ends of travel to activate the solenoid valve and hence reverse the direction of the pneumatic drive. A framework was designed and built to hold the pump components. The necessity of keeping the body of the pump immersed in the oil bath with the pneumatic cylinder outside led us to

design a mechanism based on rods and bearings (as shown in Figure 2) to provide a smooth and precise movement of the components.

The performance of the pump was tested using decane at ambient conditions in the same fashion as described previously.<sup>76</sup> With adjustment of the length of the travel to its maximum (31 mm), a displacement per cycle of 0.16 cm<sup>3</sup> was obtained measuring only the flow obtained through one channel. This equates to 76% of the theoretical displacement, and so, operating at a typical reciprocation frequency of 1 Hz, a flow rate of about 10 cm<sup>3</sup> min<sup>-1</sup> was achieved. No initial priming of the pump was necessary, and a maximum pressure head of 0.4 MPa was measured at zero flow.

Initially, a simpler system was used to take liquid samples based on a capillary connected directly to the cell. Liquid stored in the sampling capillary between analyses was prone to flash upon actuation of the valve, which caused poor reproducibility of the measurements. This was overcome by incorporating the recirculation pump.

**Analytical System.** A gas chromatograph (Shimadzu, model GC-2014) consisting of two parallel analytical lines was used for composition measurements. Figure 3 is a schematic diagram of the GC arrangement and the connection to the sampling valves. The GC oven accommodated two columns that were used in parallel. This was a benefit for separations involving components with greatly differing volatility and polarity, as in the present case, for which it is difficult to find a suitable single column. In this work we used a HayeSep Q column with 80/100 mesh (2 m × 3.2 mm o.d. × 2 mm i.d., silcosteel lined to reduce adsorption) for the separation and analysis of water and carbon dioxide. The *n*-decane however was trapped on this column at the temperature of the analysis and only eluted in a reasonable time at high temperatures ( $T \geq 470$  K). For the quantification of *n*-decane, a second packed column was used consisting of 5% OV-1 on C-WHP, with 80/100 mesh (2 m × 3.2 mm o.d. × 2 mm i.d.). Although two columns, and two injections, were required to analyze a sample, this arrangement was considered optimal for minimizing the analysis time as it permitted the use of

**Table 1.** GC Conditions for the Analysis of the Mixtures Used in This Work<sup>a</sup>

injector $\dot{V}/\text{cm}^3 \text{s}^{-1}$	oven T/K	TCD		FID	
		T/K	I/mA	T/K	$\phi$
40	483.15	373.15	503.15	90–95	503.15 1:10

<sup>a</sup> TCD = thermal conductivity detector, FID = flame ionization detector,  $\dot{V}$  = He flow rate,  $I$  = current,  $\phi$  =  $\text{H}_2/\text{air}$  flow ratio.

an isothermal program in the oven. Note that for the system (*n*-decane + carbon dioxide) only the OV-1 column alone was necessary.

The chromatograph was equipped with three detectors in series, a dual channel thermal conductivity detector (TCD), spanning both lines, and two flame ionization detectors (FID), one in each analytical line. The TCD is commonly restricted to detection of permanent gases,  $\text{CO}_2$  and water, which do not provide a signal on the FID. The FID is more sensitive to hydrocarbons and has a larger linear response range, and is the preferred one in the case of organic compounds, such as hydrocarbons, which ionize in their transit through a flame. The use of an isothermal program in the oven of the GC, as mentioned earlier, is especially beneficial in the case of the TCD, as its baseline response is affected by carrier-gas temperature and/or flow variations. The operating conditions of the GC are summarized in Table 1.

In order to minimize adsorption, the lines downstream the sampling valves leading to the gas chromatograph were siltek/sulfonert treated tubing (1.6 mm o.d., 0.8 mm i.d.) of the minimum possible length ( $\sim 0.8$  m). These lines were heated by low-voltage mineral insulated heater cables of 2.3 mm diameter (custom-made, Tempco Electric Heater Corp.) that were bound to the tubing with heat-shrinkable PTFE sleeving. K-type thermocouples were also bound to the tube to permit temperature monitoring. The tube–heater assemblies were insulated with layers of PTFE and glass fiber sleeving and encased in an outer Viton-rubber tube (11 mm o.d., 8 mm i.d.). The lines were typically operated at a temperature of about 500 K or greater. However, the short section of each line, where it passed beneath the bath fluid to join the sampling valve, was cooler at typically 430–490 K depending upon the bath temperature. Lowering the temperature of these lines to around 430 K (400 K locally) did not seem to have any effect on the reproducibility of the chromatographic peak area, as checked for the water-rich phase, but a poorer peak shape in the chromatogram was observed. The carrier gas was also preheated upstream of the sampling valves. The same treated and heated tubing was used here because of the expected expansion of the pressurized sample in the low pressure flow of carrier gas.

As a consequence of the arrangement of the GC in two analytical flow lines, additional multiport valves were required at the inlet of the chromatograph, as shown in Figure 3. One valve (Valco model DC6WE, VICI AG International) allowed the selection of the appropriate chromatographic column for the analysis of a sample. The second one (Valco model DC10WE, VICI AG International) provided the flexibility to flush the sampling system with an appropriate gas or solvent, or to create vacuum in the sampling loops before sampling, if needed. These selection valves were heated in a separated temperature-controlled enclosure operated at typically 463 K.

The GC was calibrated by an absolute method using two different procedures. The first was to use one of the multiport sampling valves. To vary the amount of carbon dioxide loaded, the equilibrium vessel was filled with the pure substance and the conditions of pressure and temperature were varied. The amounts of water and *n*-decane were each varied separately by filling the sampling loop with a solution of the pure substance in a suitable solvent. The *n*-decane was diluted with hexane whereas the water was diluted with tetrahydrofuran. The amount of the desired component was measured gravimetrically and the dilution prepared in a volumetric flask so as to prepare solutions of known concentration. These measurements of the liquid components were carried out at ambient temperature. The density of the different pure components was obtained from NIST standard reference database 69.<sup>77</sup> Both the TCD and the FID (for decane) showed linear responses to the components of interest in the range of study. The calibration was checked from time to time by a similar procedure, filling the equilibrium vessel with each pure component, and also using direct injections from gastight syringes and a precision digital syringe for the liquid components. Although it is not necessary to know accurately the volume of the sampling loop according to the first methodology used for the calibration, the complementary method using syringes was used to estimate it for subsequent comparison.

**Materials.** The  $\text{CO}_2$  used in this work was CP grade supplied by BOC with a mole-fraction purity higher than 0.99995. The *n*-decane was of a mole-fraction purity higher than 0.990 provided by Sigma-Aldrich (Dorset, U.K.). The water was deionized to an electrical resistivity  $> 18 \text{ M}\Omega \text{ cm}$  at  $T = 298 \text{ K}$  and was degassed immediately prior to use. The carrier gas used was CP-grade helium from BOC, with  $> 0.99999$  purity.

**Experimental Procedure.** The usual procedure was to clean the apparatus with appropriate solvents (typically hexane and 2-propanol) followed by flushing with gas. Then the cell was put under vacuum for a few hours to dry it. The loading of the components into the evacuated cell would typically start with the *n*-decane (using PG1 and valve V1 in Figure 1), followed by carbon dioxide (using PG2, V3 and V4), and finally, for the ternary system, water (using PG1 and V1). Since the exact amounts of each component loaded were not required, it was not necessary to clean and dry the manual syringe pump between injection of decane and water.

The measurements were isothermal. Usually the bath was left overnight to stabilize at the desired temperature. Additional injections of one of the components were used to raise the pressure, while fluid could be vented through valve V5 or drained through V2 to lower the pressure. At a chosen pressure, using only the actuation of the circulation pump (MRP in Figure 1) to promote the mass transfer, constant aqueous-phase compositions were typically measured after 10 min, although an equilibration time of  $\sim 1$  h was normally allowed. In cases of three phase equilibria, it was usual practice to start sampling first from the vapor phase (using GSV in Figure 1). The first vapor sample was always ignored, as it contained the stagnant fluid stored inside the sampling capillary. The water-rich phase was sampled next by means of the liquid sampling valve (LSV), and finally the cell was tilted to allow sampling of the middle alkane-rich phase with the same valve (LSV). For this usually a few minutes were allowed to ensure the water phase had been flushed out of the body of the pump, although due to the small dimensions and dead volume of the pump, the alkane phase could be distinguished at the outlet of the pump after just a few strokes. As a

**Table 2.** Experimental VLE Data<sup>a</sup> for (*n*-Decane (1) + Carbon Dioxide (2))

phase I		phase II	
<i>p</i> /MPa	<i>x</i> <sub>1</sub> <sup>exp</sup>	<i>p</i> /MPa	<i>y</i> <sub>1</sub> <sup>exp</sup>
<i>T</i> = 311.02 K			
2.72	0.7157	2.71	0.000 47
4.05	0.5833	4.04	0.000 44
6.15	0.3417	6.13	0.000 55
6.83	0.2417	6.82	0.000 80
7.26	0.1582	7.26	0.000 95
7.69	0.0650	7.68	0.001 48
<i>T</i> = 344.31 K			
2.51	0.8088	2.53	0.0016
3.66	0.7179	3.68	0.0024
4.44	0.6634	4.43	0.0014
6.44	0.5343	6.44	0.0017
9.04	0.3798	9.03	0.0028
10.49	0.2792	10.46	0.0061
11.52	0.2186	11.51	0.0116

<sup>a</sup> The phases are labeled as I and II for the decane-rich and CO<sub>2</sub>-rich phases, respectively.

general procedure, at least three or four samples from each phase would be taken to ensure reproducibility when there was no evidence of cross contamination or entrainment of one phase in the other during sampling. If entrainment did occur those samples would be discarded. Each measurement was performed by sending two consecutive samples, one to each column, as previously described. The time lag between consecutive chromatographic analyses for each composition measurement, consisting of two samples, was approximately 15 min. Due to the small volume of the sampling loops, the pressure drop and entrainment of low-pressure helium imposed by actuation of the sampling valves have minimal effects on the equilibrium of the system.

**Validation of the Apparatus.** The mixture (*n*-decane + carbon dioxide) was chosen to validate the apparatus through comparison with published experimental data.<sup>78–84</sup> Among these experimental data, the first experimental study was that of Reamer and Sage,<sup>78</sup> who reported VLE composition and density data for various isotherms for *T* = 277.59–510.93 K and pressures up to critical conditions using a combination of both a synthetic technique for bubble point analysis and a sampling technique mainly used for the coexisting gas phase. The reported standard error in the mole fractions was  $\pm 0.0039$ .<sup>78</sup> Nagarajan and Robinson<sup>79</sup> reported composition, density, and interfacial tension measurements on two isotherms at *T* = 344.3 K and *T* = 377.6 K at pressures up to the critical point of the mixture using an analytical-type apparatus with recirculation of either vapor or liquid through sampling valves and online chromatographic analysis. In the study of Chou et al.<sup>80</sup> composition measurements at *T* = 344.25 K and *T* = 377.55 K were reported; an analytical-type apparatus with recirculation of the vapor phase and off-line GC analysis was used with a reported reproducibility between samples within  $\pm 0.04x$  for liquid and  $\pm 0.02y$  for vapor and estimated uncertainties of  $\pm 0.005$  and  $\pm 0.002$ , respectively, for liquid and vapor mole fractions. Han et al.<sup>81</sup> presented

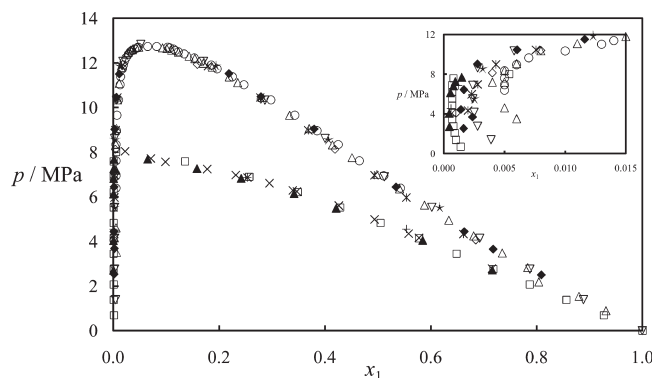


**Figure 4.** Isothermal pressure–composition (*p*, *x*) phase diagram for the (*n*-decane (1) + carbon dioxide (2)) system at *T* = 311.0 K and *T* = 344.3 K. The filled symbols represent the data gathered during this work ( $\blacktriangle$  at *T* = 311.02 K and  $\blacklozenge$  at *T* = 344.31 K). The open symbols correspond to published experimental VLE phase equilibria at the isotherms:  $\square$ , *T* = 310.93 K;<sup>78</sup>  $\times$ , *T* = 310.95 K;<sup>81</sup>  $+$ , *T* = 311.0 K;<sup>82</sup>  $\nabla$ , *T* = 344.3 K;<sup>78</sup>  $\circ$ , *T* = 344.26 K;<sup>79</sup>  $\diamond$ , *T* = 344.25 K;<sup>80</sup>  $\star$ , *T* = 344.3 K;<sup>82</sup>  $*$ , *T* = 344.25 K;<sup>83</sup> and  $\Delta$ , *T* = 344.3 K.<sup>84</sup>

composition and density measurements for this system at *T* = 310.95 K and up to the critical pressure using an analytical technique with circulation of the gas and off-line analysis using sample cells as in the previous study; only the saturated liquid-phase compositions were reported. A few composition measurements were also presented by Iwai et al.<sup>82</sup> at *T* = 311.0 K and *T* = 344.3 K using an analytical apparatus in which both liquid and vapor were recirculated through their respective sampling valves. They reported a standard deviation in composition lower than 0.000 082. Jennings and Schucker<sup>83</sup> reported composition measurements at *T* = 344.25 K with a reproducibility for liquid and vapor mole fractions of  $\pm 0.0013$  and  $\pm 0.000 07$ , respectively, using an analytical flow-type apparatus. The same equipment as Nagarajan and Robinson<sup>79</sup> with some modifications was used by Shaver et al.<sup>84</sup> to obtain composition, density, and interfacial tension data at *T* = 344.3 K and pressures up to the critical point with a reported accuracy in mole fraction of  $\pm 0.003$  and an estimated precision of 0.0005 for both phases.

Experimental VLE measurements on the same system were obtained by us on two isotherms at *T* = 311.0 K and *T* = 344.3 K. The results are collected in Table 2, and the comparison with the literature is presented in Figure 4. Good agreement is found at both temperatures for liquid and vapor phases, although some discrepancies are seen among the vapor phase data reported by different authors. This is seen at *T* = 344.3 K, where the mole fraction of decane in the vapor phase at pressures of about 4 MPa varies from a minimum of *y* = 0.001<sup>80</sup> to *y* = 0.005.<sup>84</sup> In this latter study, Shaver et al.<sup>84</sup> reported difficulty in replicating vapor sampling analysis at low pressure, but it was said to be overcome at pressures higher than 3.5 MPa. Similarly, higher mole fractions of decane in the vapor phase were also reported by Nagarajan and Robinson<sup>79</sup> as seen in Figure 4, using the older version of the same equipment where the minimum pressure reported was about 6 MPa.

Our measurements on the binary system were obtained using direct sampling of the liquid phase through a capillary. Recirculation had not been implemented at that stage, and the rocking mechanism was the means to promote mass transfer. A large number of samples (typically more than 10) was needed in this

**Table 3. Experimental VLLE Data<sup>a</sup> for (*n*-Decane(1) + Carbon Dioxide(2) + Water(3))**

phase	<i>p</i> /MPa	<i>x</i> <sub>1</sub> <sup>exp</sup>	<i>x</i> <sub>2</sub> <sup>exp</sup>	<i>x</i> <sub>3</sub> <sup>exp</sup>	<i>p</i> /MPa	<i>x</i> <sub>1</sub> <sup>pred</sup>	<i>x</i> <sub>2</sub> <sup>pred</sup>	<i>x</i> <sub>3</sub> <sup>pred</sup>
<i>T</i> = 323.08 K								
I	2.09	0.8177	0.1802	0.0021	2.10	0.7351	0.2628	0.0020
II	2.12	0.0011	0.9940	0.0049	2.10	0.0006	0.9925	0.0069
III	2.11	4.4 × 10 <sup>-7</sup>	0.0069	0.9931	2.10	3.6 × 10 <sup>-18</sup>	0.0058	0.9942
I	4.77	0.5813	0.4153	0.0035	4.77	0.4990	0.4986	0.0024
II	4.78	0.0010	0.9963	0.0028	4.77	0.0005	0.9956	0.0039
III	4.77	4.0 × 10 <sup>-7</sup>	0.0134	0.9866	4.77	4.0 × 10 <sup>-18</sup>	0.0124	0.9876
I	7.05	0.3824	0.6135	0.0041	7.05	0.3357	0.6613	0.0030
II	7.05	0.0039	0.9937	0.0023	7.05	0.0006	0.9960	0.0034
III	7.05	5.0 × 10 <sup>-7</sup>	0.0173	0.9827	7.05	4.0 × 10 <sup>-18</sup>	0.0170	0.9830
I	8.46	0.2326	0.7627	0.0047	8.50	0.2303	0.7658	0.0039
II	8.50	0.0041	0.9934	0.0025	8.50	0.0008	0.9958	0.0034
III	8.54	5.3 × 10 <sup>-7</sup>	0.0190	0.9810	8.50	3.7 × 10 <sup>-18</sup>	0.0195	0.9805
<i>T</i> = 353.11 K								
I	0.94	0.9259	0.0640	0.0101	0.94	0.9046	0.0895	0.0059
II	0.94	0.0054	0.9594	0.0352	0.94	0.0047	0.9427	0.0526
III	0.95	1.9 × 10 <sup>-6</sup>	0.0021	0.9979	0.94	1.5 × 10 <sup>-16</sup>	0.0019	0.9981
I	1.98	0.8535	0.1398	0.0067	2.01	0.8109	0.1832	0.0059
II	1.99	0.0031	0.9713	0.0256	2.01	0.0026	0.9709	0.0265
III	2.05	1.5 × 10 <sup>-6</sup>	0.0043	0.9956	2.01	1.6 × 10 <sup>-16</sup>	0.0042	0.9958
I	4.62	0.6776	0.3151	0.0072	4.64	0.6258	0.3680	0.0062
II	4.64	0.0024	0.9851	0.0124	4.64	0.0018	0.9843	0.0139
III	4.66	1.0 × 10 <sup>-6</sup>	0.0091	0.9909	4.64	1.8 × 10 <sup>-16</sup>	0.0093	0.9907
I	6.99	0.5324	0.4595	0.0082	7.02	0.4944	0.4988	0.0068
II	7.02	0.0038	0.9870	0.0092	7.02	0.0019	0.9869	0.0112
III	7.04	9.0 × 10 <sup>-7</sup>	0.0125	0.9875	7.02	1.9 × 10 <sup>-16</sup>	0.0134	0.9866
I	9.58	0.3796	0.6073	0.0132	9.62	0.3740	0.6183	0.0077
II	9.62	0.0055	0.9869	0.0076	9.62	0.0024	0.9873	0.0103
III	9.64	8.6 × 10 <sup>-7</sup>	0.0157	0.9843	9.62	2.0 × 10 <sup>-16</sup>	0.0172	0.9828
I	12.13	0.2325	0.7534	0.0141	12.15	0.2683	0.7224	0.0092
II	12.17	0.0133	0.9795	0.0072	12.15	0.0037	0.9856	0.0107
III	12.16	7.1 × 10 <sup>-7</sup>	0.0184	0.9816	12.15	2.0 × 10 <sup>-16</sup>	0.0203	0.9797
I	13.34	0.1442	0.8426	0.0132	13.35	0.2178	0.7718	0.0104
II	13.36	0.0288	0.9629	0.0083	13.35	0.0050	0.9837	0.0113
III	13.34	1.2 × 10 <sup>-6</sup>	0.0192	0.9808	13.35	1.9 × 10 <sup>-16</sup>	0.0215	0.9785
<i>T</i> = 373.07 K								
I	1.06	0.9148	0.0639	0.0213	1.06	0.9095	0.0795	0.0110
II	1.06	0.0138	0.8940	0.0922	1.06	0.0097	0.8904	0.0998
III	1.06	1.7 × 10 <sup>-6</sup>	0.0018	0.9982	1.06	1.6 × 10 <sup>-15</sup>	0.0018	0.9982
I	1.99	0.8575	0.1269	0.0156	2.00	0.8393	0.1497	0.0110
II	2.00	0.0074	0.9410	0.0516	2.00	0.0059	0.9380	0.0561
III	2.00	1.2 × 10 <sup>-6</sup>	0.0035	0.9965	2.00	1.7 × 10 <sup>-15</sup>	0.0036	0.9964
I	2.96	0.7965	0.1898	0.0137	2.98	0.7735	0.2154	0.0111
II	2.98	0.0049	0.9557	0.0394	2.98	0.0046	0.9554	0.0400
III	2.98	8.3 × 10 <sup>-7</sup>	0.0053	0.9947	2.98	1.7 × 10 <sup>-15</sup>	0.0054	0.9946
I	3.88	0.7387	0.2459	0.0154	3.89	0.7180	0.2709	0.0112
II	3.90	0.0054	0.9677	0.0269	3.89	0.0041	0.9635	0.0325
III	3.88	1.3 × 10 <sup>-6</sup>	0.0066	0.9934	3.89	1.8 × 10 <sup>-15</sup>	0.0070	0.9930
I	5.02	0.6718	0.3083	0.0199	5.03	0.6547	0.3339	0.0114
II	5.01	0.0051	0.9680	0.0269	5.03	0.0038	0.9692	0.0271
III	5.05	1.4 × 10 <sup>-6</sup>	0.0085	0.9915	5.03	1.9 × 10 <sup>-15</sup>	0.0089	0.9911
I	6.51	0.5933	0.3860	0.0207	6.49	0.5821	0.4062	0.0117
II	6.49	0.0062	0.9741	0.0197	6.49	0.0037	0.9731	0.0232
<i>T</i> = 373.10 K								

Table 3. Continued

phase	$p/\text{MPa}$	$x_1^{\text{exp}}$	$x_2^{\text{exp}}$	$x_3^{\text{exp}}$	$p/\text{MPa}$	$x_1^{\text{pred}}$	$x_2^{\text{pred}}$	$x_3^{\text{pred}}$
III	6.47	$8.6 \times 10^{-7}$	0.0105	0.9895	6.49	$2.0 \times 10^{-15}$	0.0112	0.9888
I	7.90	0.5196	0.4592	0.0212	7.91	0.5188	0.4691	0.0121
II	7.93	0.0062	0.9769	0.0169	7.91	0.0039	0.9751	0.0210
III	7.91	$1.4 \times 10^{-6}$	0.0128	0.9872	7.91	$2.1 \times 10^{-15}$	0.0133	0.9867
I	9.15	0.4641	0.5150	0.0209	9.14	0.4687	0.5188	0.0125
II	9.14	0.0119	0.9719	0.0162	9.14	0.0041	0.9759	0.0199
III	9.13	$1.0 \times 10^{-6}$	0.0136	0.9864	9.14	$2.1 \times 10^{-15}$	0.0151	0.9849
I	10.96	0.3792	0.5985	0.0250	10.95	0.4010	0.5856	0.0134
II	10.97	0.0144	0.9693	0.0163	10.95	0.0048	0.9760	0.0192
III	10.94	$7.3 \times 10^{-7}$	0.0154	0.9846	10.95	$2.2 \times 10^{-15}$	0.0174	0.9826
I	12.72	0.2956	0.6777	0.0267	12.74	0.3396	0.6460	0.0144
II	12.75	0.0146	0.9709	0.0144	12.74	0.0059	0.9749	0.0191
III	12.76	$6.2 \times 10^{-7}$	0.0165	0.9835	12.74	$2.2 \times 10^{-15}$	0.0195	0.9805
I	14.70	0.1975	0.7747	0.0278	14.72	0.2752	0.7088	0.0159
II	14.75	0.0330	0.9517	0.0153	14.72	0.0080	0.9721	0.0198
III	14.74	$5.3 \times 10^{-7}$	0.0177	0.9823	14.72	$2.2 \times 10^{-15}$	0.0215	0.9785
I	15.26	0.1628	0.8087	0.0285	15.28	0.2574	0.7261	0.0165
II	15.29	0.0431	0.9413	0.0157	15.28	0.0089	0.9709	0.0202
III	15.27	$7.0 \times 10^{-7}$	0.0183	0.9817	15.28	$2.2 \times 10^{-15}$	0.0220	0.9780
$T = 393.14 \text{ K}$					$T = 393.15 \text{ K}$			
I	0.88	0.9314	0.0401	0.0285	0.88	0.9325	0.0483	0.0192
II	0.88	0.0259	0.7812	0.1929	0.88	0.0239	0.7442	0.2319
III	0.88	$6.0 \times 10^{-6}$	0.0013	0.9987	0.88	$1.4 \times 10^{-14}$	0.0012	0.9988
I	2.08	0.8626	0.1100	0.0275	2.08	0.8534	0.1274	0.0192
II	2.09	0.0129	0.8963	0.0908	2.08	0.0119	0.8833	0.1048
III	2.08	$3.1 \times 10^{-6}$	0.0030	0.9970	2.08	$1.5 \times 10^{-14}$	0.0033	0.9967
I	3.29	0.7960	0.1752	0.0288	3.30	0.7818	0.1989	0.0193
II	3.32	0.0095	0.9295	0.0610	3.30	0.0088	0.9205	0.0707
III	3.31	$1.9 \times 10^{-6}$	0.0047	0.9953	3.30	$1.6 \times 10^{-14}$	0.0053	0.9947
I	4.70	0.7153	0.2552	0.0295	4.71	0.7081	0.2725	0.0195
II	4.73	0.0081	0.9463	0.0456	4.71	0.0075	0.9389	0.0537
III	4.72	$1.9 \times 10^{-6}$	0.0068	0.9932	4.71	$1.7 \times 10^{-14}$	0.0076	0.9924
I	6.03	0.6477	0.3191	0.0332	6.02	0.6466	0.3337	0.0197
II	6.02	0.0097	0.9542	0.0361	6.02	0.0070	0.9477	0.0453
III	6.02	$4.5 \times 10^{-6}$	0.0086	0.9914	6.02	$1.7 \times 10^{-14}$	0.0096	0.9904
I	7.54	0.5859	0.3795	0.0346	7.58	0.5807	0.3992	0.0201
II	7.64	0.0078	0.9605	0.0317	7.58	0.0069	0.9535	0.0396
III	7.57	$2.7 \times 10^{-6}$	0.0107	0.9893	7.58	$1.8 \times 10^{-14}$	0.0119	0.9881
I	9.54	0.4857	0.4821	0.0322	9.59	0.5051	0.4740	0.0209
II	9.63	0.0112	0.9636	0.0252	9.59	0.0073	0.9572	0.0355
III	9.59	$2.6 \times 10^{-6}$	0.0127	0.9873	9.59	$1.9 \times 10^{-14}$	0.0146	0.9854
I	11.78	0.4006	0.5660	0.0334	11.81	0.4308	0.5473	0.0220
II	11.87	0.0184	0.9569	0.0247	11.81	0.0084	0.9583	0.0333
III	11.80	$8.3 \times 10^{-7}$	0.0145	0.9855	11.81	$2.0 \times 10^{-14}$	0.0174	0.9826
I	14.78	0.2880	0.6752	0.0367	14.83	0.3409	0.6351	0.0240
II	14.88	0.0299	0.9474	0.0227	14.83	0.0110	0.9562	0.0328
III	14.85	$1.0 \times 10^{-6}$	0.0169	0.9831	14.83	$2.1 \times 10^{-14}$	0.0208	0.9792
I	16.65	0.1895	0.7736	0.0369	16.70	0.2894	0.6849	0.0257
II	16.72	0.0542	0.9218	0.0240	16.70	0.0137	0.9527	0.0335
III	16.74	$1.0 \times 10^{-6}$	0.0181	0.9819	16.70	$2.2 \times 10^{-14}$	0.0226	0.9774
$T = 413.16 \text{ K}$					$T = 413.15 \text{ K}$			
I	0.95	0.9275	0.0312	0.0414	0.96	0.9323	0.0358	0.0319
II	0.95	0.0443	0.6203	0.3354	0.96	0.0426	0.5716	0.3859
III	0.96	$7.0 \times 10^{-6}$	0.0010	0.9990	0.96	$1.1 \times 10^{-13}$	0.0009	0.9991

**Table 3. Continued**

phase	<i>p</i> /MPa	<i>x</i> <sub>1</sub> <sup>exp</sup>	<i>x</i> <sub>2</sub> <sup>exp</sup>	<i>x</i> <sub>3</sub> <sup>exp</sup>	<i>p</i> /MPa	<i>x</i> <sub>1</sub> <sup>pred</sup>	<i>x</i> <sub>2</sub> <sup>pred</sup>	<i>x</i> <sub>3</sub> <sup>pred</sup>
I	3.19	0.8095	0.1483	0.0422	3.20	0.8066	0.1617	0.0317
II	3.20	0.0170	0.8778	0.1052	3.20	0.0166	0.8540	0.1294
III	3.21	5.5 × 10 <sup>-6</sup>	0.0042	0.9958	3.20	1.2 × 10 <sup>-13</sup>	0.0046	0.9954
I	4.91	0.7220	0.2337	0.0442	4.93	0.7238	0.2443	0.0319
II	4.94	0.0136	0.9131	0.0734	4.93	0.0133	0.8951	0.0916
III	4.94	4.3 × 10 <sup>-6</sup>	0.0064	0.9936	4.93	1.3 × 10 <sup>-13</sup>	0.0073	0.9927
I	7.43	0.6102	0.3449	0.0449	7.47	0.6192	0.3483	0.0324
II	7.51	0.0161	0.9213	0.0626	7.47	0.0119	0.9190	0.0691
III	7.52	5.8 × 10 <sup>-6</sup>	0.0097	0.9903	7.47	1.4 × 10 <sup>-13</sup>	0.0110	0.9890
I	10.24	0.4981	0.4532	0.0486	10.30	0.5204	0.4461	0.0335
II	10.29	0.0188	0.9343	0.0469	10.30	0.0123	0.9293	0.0584
III	10.30	4.3 × 10 <sup>-6</sup>	0.0129	0.9871	10.30	1.6 × 10 <sup>-13</sup>	0.0149	0.9851
I	13.30	0.3859	0.5675	0.0465	13.30	0.4301	0.5346	0.0353
II	13.26	0.0263	0.9334	0.0404	13.30	0.0141	0.9322	0.0537
III	13.29	2.7 × 10 <sup>-6</sup>	0.0156	0.9844	13.30	1.7 × 10 <sup>-13</sup>	0.0186	0.9814
I	17.07	0.2282	0.7190	0.0528	17.10	0.3299	0.6316	0.0385
II	17.16	0.0600	0.9043	0.0357	17.10	0.0189	0.9286	0.0526
III	17.08	1.6 × 10 <sup>-6</sup>	0.0180	0.9820	17.10	1.8 × 10 <sup>-13</sup>	0.0226	0.9774

<sup>a</sup>The phases are labeled as I, II, and III for the decane-rich, CO<sub>2</sub>-rich, and water-rich phases, respectively.

arrangement to obtain a satisfactory standard deviation in the liquid-phase mole fraction. The typical standard deviations for the liquid were the following:  $\sigma_x = 8 \times 10^{-3}$  and  $\sigma_x = 1 \times 10^{-2}$  for the liquid phases and  $\sigma_y = 3 \times 10^{-5}$  and  $\sigma_y = 4 \times 10^{-4}$  for the gas phases at  $T = 311.0$  K and  $T = 344.3$  K, respectively. The improvements in the repeatability of the liquid-phase measurements after incorporating the circulation pump are discussed in the next section for the ternary system.

**Experimental Results for (*n*-Decane + Carbon Dioxide + Water).** The experiments performed during this work for (*n*-decane + carbon dioxide + water) were mainly focused on regions of three-phase VLLE equilibria. In Table 3, we report the experimental three-phase data measured at  $T = (413, 393, 373, 353,$  and  $323)$  K. At each temperature we have also observed and measured the critical point between the decane-rich and the CO<sub>2</sub>-rich phases. These data appear in Table 4, and the measurements will be discussed in detail in the next section.

The standard uncertainty in the composition measurements was calculated on the basis of estimations of the contributions corresponding to calibration of the chromatograph, pressure, and temperature measurements, as<sup>85</sup>

$$u_c^2(x_i) = \left( \frac{\partial x_i}{\partial p} \right)^2 u^2(p) + \left( \frac{\partial x_i}{\partial T} \right)^2 u^2(T) + \sum_{j=1}^3 \left( \frac{\partial x_i}{\partial n_j} \frac{\partial n_j}{\partial A_j} \right)^2 u^2(A_j) \quad (1)$$

where  $u_c(x_i)$  is the combined standard uncertainty in the composition,  $u(A_j)$  is the standard uncertainty related to the calibration of the chromatograph for component  $j$ ,  $u(p) = 10$  kPa, and  $u(T) = 0.05$  K. The relative standard uncertainties from the chromatographic calibrations were below 2% for each of the three components. In practice, the combined standard uncertainty in the composition measurements varied depending on the component and the phase in question; the results are summarized in Table 5.

**Table 4. Experimental LLE Data for (*n*-Decane (1) + Carbon Dioxide (2) + Water (3)) at the Critical Point between the Decane-Rich and CO<sub>2</sub>-Rich Phases<sup>a</sup>**

T/K	<i>p</i> /MPa	phase II			phase III		
		<i>x</i> <sub>1</sub> <sup>exp</sup>	<i>x</i> <sub>2</sub> <sup>exp</sup>	<i>x</i> <sub>3</sub> <sup>exp</sup>	<i>x</i> <sub>1</sub> <sup>exp</sup>	<i>x</i> <sub>2</sub> <sup>exp</sup>	<i>x</i> <sub>3</sub> <sup>exp</sup>
323.10	9.62	0.0226	0.9701	0.0073	1.3 × 10 <sup>-6</sup>	0.0204	0.9796
353.12	13.79	0.0759	0.9089	0.0152	1.6 × 10 <sup>-6</sup>	0.0198	0.9802
373.11	15.81	0.0944	0.8781	0.0275	5.0 × 10 <sup>-7</sup>	0.0187	0.9813
393.13	17.30	0.1209	0.8414	0.0378	8.1 × 10 <sup>-7</sup>	0.0187	0.9813
413.15	18.12	0.1132	0.8323	0.0545	8.4 × 10 <sup>-7</sup>	0.0195	0.9805

<sup>a</sup>The combination of both phases is referred here as CO<sub>2</sub>-rich phase. The phases are labelled as II and III for the CO<sub>2</sub>-rich and the water-rich phases, respectively.

A second class of uncertainty is that derived from the repeatability of the measurements as a result of random sources of error. This has been quantified in terms of standards deviations

$$\sigma_{x_i} = \left( \frac{\sum_{i=1}^N (x_i - \bar{x}_i)^2}{N-1} \right)^{1/2} \quad (2)$$

calculated for every state point and then averaged. These standard deviations in composition are also presented in Table 5. The overall uncertainty obtained combining eqs 1 and 2 is also considered and denoted as  $u(x_i)$  in Table 5.

## ■ MODELS, THEORY, AND CALCULATIONS

The choice of the states to be measured was guided by theoretical calculations. Accurate equations of state allow such a procedure, and this was one reason we used SAFT-VR in this work. To model the components of interest, a number of intermolecular potential parameters need to be determined. Within the SAFT-VR

**Table 5.** Combined Standard Uncertainty  $u_c(x_i)$ , Standard Deviations  $\sigma_{xi}$ , and Overall Uncertainty  $u(x_i)$  for the Composition Measurements of the System (*n*-Decane(1) + Carbon Dioxide (2) + Water (3)) in Mole Fraction<sup>a</sup>

	phase I			phase II			phase III		
	$x_1$	$x_2$	$x_3$	$x_1$	$x_2$	$x_3$	$x_1$	$x_2$	$x_3$
$u_c(x_i)$	$4 \times 10^{-3}$	$4 \times 10^{-3}$	$1 \times 10^{-3}$	$4 \times 10^{-4}$	$2 \times 10^{-3}$	$2 \times 10^{-3}$	$2 \times 10^{-7}$	$2 \times 10^{-4}$	$2 \times 10^{-4}$
$\sigma_{xi}$	$3 \times 10^{-3}$	$2 \times 10^{-3}$	$3 \times 10^{-3}$	$5 \times 10^{-4}$	$2 \times 10^{-3}$	$2 \times 10^{-3}$	$7 \times 10^{-7}$	$2 \times 10^{-4}$	$2 \times 10^{-4}$
$u(x_i)$	$5 \times 10^{-3}$	$4 \times 10^{-3}$	$3 \times 10^{-3}$	$6 \times 10^{-4}$	$3 \times 10^{-3}$	$2 \times 10^{-3}$	$8 \times 10^{-7}$	$3 \times 10^{-4}$	$3 \times 10^{-4}$

<sup>a</sup> The phases are labelled as I, II, and III for the decane-rich, CO<sub>2</sub>-rich, and water-rich phases, respectively.

formalism,<sup>37,38</sup> molecules are modeled as associating chains of segments interacting through attractive potentials of variable range. In this work we consider chains of  $m_i$  tangent spheres of diameter  $\sigma_{ii}$  that interact through square-well potentials of well-depth  $\varepsilon_{ii}$  and range  $\lambda_{ii}$ . Hydrogen bonding interactions are mediated by adding short-range off-center associating sites to the molecules. These interact through attractive square-well potentials of energy  $\varepsilon_{ii}^{\text{HB}}$  and cutoff range  $r_{ci,ii}$ ; each of these sites is placed at a distance  $r_{di,ii}/\sigma_{ii} = 0.25$  from the center of the segment.

**Pure Components.** The models used here for the pure components are based on previous work. Decane was modeled as a homonuclear chain comprising four segments based on a previous parametrization for the alkane family.<sup>86</sup> CO<sub>2</sub> was modeled as a nonassociating molecule comprising two spherical segments,<sup>72,73</sup> and water was modeled as a single sphere with four off-center square-well association sites, as this was found to be the most appropriate model to describe the hydrogen bonding based on spectroscopic data.<sup>87</sup> The optimized SAFT-VR parameters for the pure components are presented in Table 6 for completeness. These intermolecular parameters were determined by comparison to experimental vapor pressure and liquid density data for the pure components in the region from the triple point temperature to 90% of the critical temperature.

**Mixtures.** To study the behavior of mixtures, a number of unlike interactions, or cross parameters, need to be determined. In the simplest analysis, arithmetic and geometric-mean rules using the pure components parameters can be applied. The unlike diameter is given by

$$\sigma_{ij} = \frac{\sigma_{ii} + \sigma_{jj}}{2} \quad (3)$$

and is exact for hard-core potentials such as the square-well used here. Unfortunately, the application of simple combining rules for the unlike depth  $\varepsilon_{ij}$  and the range  $\lambda_{ij}$  of the square-well potential rarely lead to good predictions of the mixture phase behavior. Adjustable parameters need to be included as follows:

$$\lambda_{ij} = (1 - \gamma_{ij}) \frac{\lambda_{ii}\sigma_{ii} + \lambda_{jj}\sigma_{jj}}{\sigma_{ii} + \sigma_{jj}} \quad (4)$$

and

$$\varepsilon_{ij} = (1 - k_{ij}) \sqrt{(\varepsilon_{ii}\varepsilon_{jj})} \quad (5)$$

These parameters  $\gamma_{ij}$  and  $k_{ij}$  typically need to be estimated by comparison with experimental mixture data. In this work a common arithmetic-mean rule is used for  $\lambda_{ij}$  so that  $\gamma_{ij} = 0$  in eq 4. The strong nonideality of the systems studied here, together with differences in molecular size, makes it necessary to go beyond the simple geometric-mean or Berthelot rule for  $\varepsilon_{ij}$ . This combining rule can be extended by including the effects of

**Table 6.** SAFT-VR Parameters<sup>a</sup> Used for Modelling the Behavior of the Pure Components

	ref	$m_i$	$\sigma_{ii}/\text{\AA}$	$(\varepsilon_{ii}/k_B)/\text{K}$	$\lambda_{ii}$	$(\varepsilon_{ii}^{\text{HB}}/k_B)/\text{K}$	$r_{ci,ii}/\text{\AA}$
CO <sub>2</sub>	72, 73	2.0	2.7864	179.27	1.5157		
<i>n</i> -decane	86	4.0	3.9675	247.08	1.5925		
H <sub>2</sub> O	87	1.0	3.0342	250.00	1.7889	1400.00	2.10822

<sup>a</sup>  $m_i$  is the number of square-well segments in the molecule,  $\sigma_{ii}$  is the hard-core diameter,  $\lambda_{ii}$  and  $\varepsilon_{ii}$  are the range and the depth of the square-well potential, and  $\varepsilon_{ii}^{\text{HB}}$  and  $r_{ci,ii}$  are those of the hydrogen-bonding interaction.

differences in ionization potentials and molecular sizes through consideration of the London theory of dispersion interactions. This was done originally by Hudson and McCoubrey for the Lennard-Jones potential.<sup>57</sup> Recently, a method for generalizing the combining rule obtained by Hudson and McCoubrey to a square-well intermolecular potential has been presented.<sup>58</sup> The use of this combining rule leads to a temperature- and phase-independent value for the  $k_{ij}$  binary-interaction parameter only when dispersion interactions alone are considered. Extended expressions for the  $k_{ij}$  applicable to polar molecules are also given in ref 58 including interactions such as dipole–dipole and dipole–induced-dipole, as well those arising from the permanent quadrupole moment of the molecules. In the absence of dipole and hydrogen-bonding terms the  $k_{ij}$  is given by<sup>58</sup>

$$k_{ij} = 1 - \left\{ \frac{3}{m_i m_j \sigma_{ij}^3 (\lambda_{ij}^3 - 1)} \times \left( \frac{1}{2\sigma_{ij}^3 (4\pi\epsilon_r \epsilon_0)^2} \frac{I_i I_j}{(I_i + I_j)} \alpha_{0,i}^* \alpha_{0,j}^* \right. \right. \\ \left. \left. + \frac{1}{5\sigma_{ij}^5 (4\pi\epsilon_r \epsilon_0)^2} \frac{3}{2} (Q_i^2 \alpha_{0,j}^* + Q_j^2 \alpha_{0,i}^*) \right) \frac{1}{\sqrt{(\varepsilon_{ii} \varepsilon_{jj})}} \right\} \quad (6)$$

where  $\epsilon_0$  is the permittivity of vacuum,  $\epsilon_r$  is the relative permittivity (or dielectric constant) of the media,  $I_i$  and  $I_j$  are the ionization potentials of the molecules,  $\alpha_{0,i}$  and  $\alpha_{0,j}$  are the electronic polarizabilities, and  $Q_i$  and  $Q_j$  are the total quadrupole moments. The electronic polarizabilities  $\alpha_{0,i}^*$  and  $\alpha_{0,j}^*$  are obtained using an equivalent expression for the like–like interactions.

The resulting combining rule for polar molecules<sup>58</sup> leads to a value for the  $k_{ij}$  parameter that is temperature-dependent and also phase-dependent on the basis of differences in the dielectric constant of each phase and the dipole moments of each species. Here we avoid considering a temperature-dependent  $k_{ij}$ , thus simplifying the use of the theory. We also consider a unique phase-independent  $k_{ij}$  to be able to predict critical points.

*(n-Decane + Carbon Dioxide).* The extension of the Hudson and McCoubrey combining rules<sup>58</sup> was used here to calculate an appropriate value for the  $k_{ij}$  of the system (*n*-decane + carbon

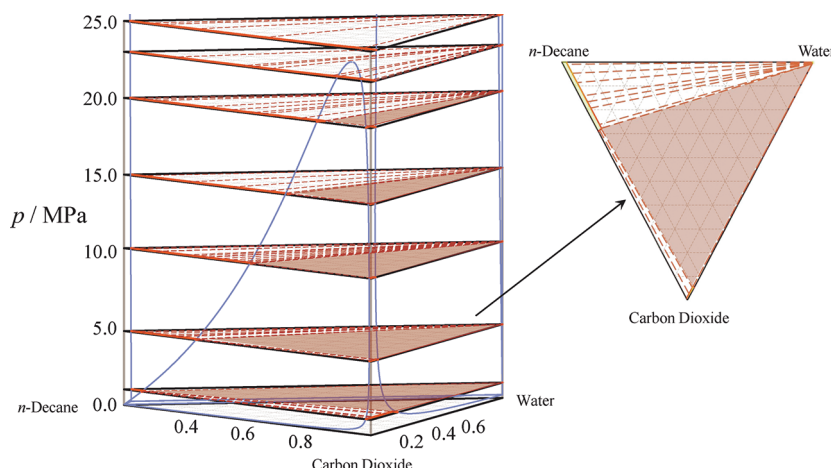


**Figure 5.** Isothermal pressure–composition ( $p, x$ ) prismatic diagram for the (*n*-decane + carbon dioxide + water) system at  $T = 393.15\text{ K}$  calculated with SAFT-VR. Regions of three-phase equilibria appear colored in light red. Regions of two-phase equilibria appear delimited by continuous thick red lines. Small regions of one-phase equilibria appear in yellow in the outer regions delimited by the continuous thick red curves. The two-phase coexisting regions for the binary subsystems appear in the lateral sides of the prismatic diagram with a continuous blue line. Insert: detail showing the isobar at  $p = 5\text{ MPa}$ .

dioxide) with SAFT-VR. The  $\text{CO}_2$  molecule because of its symmetry does not have net electrical dipole moment, but it has an important quadrupole moment. The effect of considering the quadrupole moment for the  $\text{CO}_2$  modifies slightly the value calculated for the  $k_{ij}$ , making it phase and temperature dependent through terms involving the dielectric constant of the media. However, the dielectric constant of both liquid decane and liquid  $\text{CO}_2$  are close to that for the vapor (~unity) for the temperatures of study<sup>88</sup> (as a comparison, the dielectric constant for liquid water is ~80 at  $T = 293\text{ K}$ <sup>88</sup>) which leads to a negligible effect of temperature and density. A value for the dielectric constant  $\epsilon_r = 1$  was used in this work leading to  $k_{ij} = 0.1276$  using eq 6. This was calculated using a value for the quadrupole moment of  $\text{CO}_2$ :  $Q = -1.4 \times 10^{-39}\text{ C m}^2$  and ionization potentials<sup>88</sup>  $I = 1.5 \times 10^{-18}\text{ J}$  and  $I = 2.2 \times 10^{-18}\text{ J}$  for decane and  $\text{CO}_2$ , respectively.

**Aqueous Systems.** To model aqueous systems we have opted to fit to mixture data for the range of temperatures and pressures of interest with a single temperature- and phase-independent parameter. The fitted parameter,  $k_{ij} = -0.06$ , for the ( $\text{carbon dioxide} + \text{water}$ ) system taken from a previous work<sup>69</sup> was obtained using experimental data over a temperature range 273–373 K and pressures 0.007–10 MPa. For the (*n*-decane + water) system, the value  $k_{ij} = 0.2725$  was obtained by fitting to compositions belonging to the vapor–liquid region and the saturated decane-rich phase in the liquid–liquid region at temperatures 473–523 K and pressures 0.1–75 MPa on the basis of the availability of data.<sup>90,91</sup>

**Study of the Three-Phase Equilibria of (*n*-Decane + Carbon Dioxide + Water).** The calculations of the phase behavior for the ternary system were carried out using the ( $p, T$ ) flash algorithm of Pereira et al.,<sup>92,93</sup> a reliable algorithm able to provide the number of stable fluid phases at equilibrium along with their properties without the need of initial guesses. The calculated critical point overpredicts the experimental one, as with any classical equation of state based on mean-field theory. Although crossover treatments have already been applied to SAFT-VR to correct for this behavior,<sup>94–97</sup> here we do not make use of such methods.

The immiscibility of the binary systems comprising the (*n*-decane + carbon dioxide + water) mixture dictates that a

large part of the diagram will be occupied by a region of three phase equilibria. This is observed in Figure 5 where calculations at  $T = 393.15\text{ K}$  performed with SAFT-VR and the chosen models are presented. Large regions of two- and three-phase equilibria are observed, and only very small regions of single-phase equilibria which appear in the margins of the diagram are seen. As can be observed, the area of three-phase coexistence decreases as the pressure increases. There is a limiting pressure or critical pressure at which the carbon-dioxide-rich and the decane-rich phases become miscible, and two coexisting phases are observed from there on. At low pressure, the subsystem (*n*-decane + water) exhibits a point of three-phase equilibria, which is also depicted in the diagram.

In Table 3 the experimental three-phase VLLE measurements are compared to the calculations performed with SAFT-VR. The temperature for the calculations is within experimental uncertainty; the choice of pressure is an average of the experimental measurements at each equilibrium state. To offer a visual comparison with the theory, we have collected some of the data for four isotherms and plotted them in Figure 6. These triangular diagrams are projections onto a plane of isobaric slices through a prismatic diagram such as Figure 5. As can be seen in Figure 5, the three-phase region for a given pressure diminishes as the critical point between the  $\text{CO}_2$ -rich and decane-rich phases is approached. Through a comparison of the plots in Figure 6, the reduction of these regions of immiscibility with temperature is also apparent. Data at the lowest temperature of 323 K, which shows the poorest miscibility from all the five isotherms studied, is not represented in this figure for the sake of brevity. As the pressure of the system is increased, if the three phase coexistence area of the diagram is followed, a single critical point between the  $\text{CO}_2$ -rich and decane-rich phases in the presence of a water-rich phase can be found. This point can be observed visually in the experiment as a colorful critical opalescence changing from yellow to an intense red, finally becoming opaque at the critical point. The composition at this point was measured at a very slightly higher pressure, achieved by injecting water. In Figure 7 we plot the observed critical locus as a function of temperature (cf. Table 4). These results are not compared here with the calculations performed

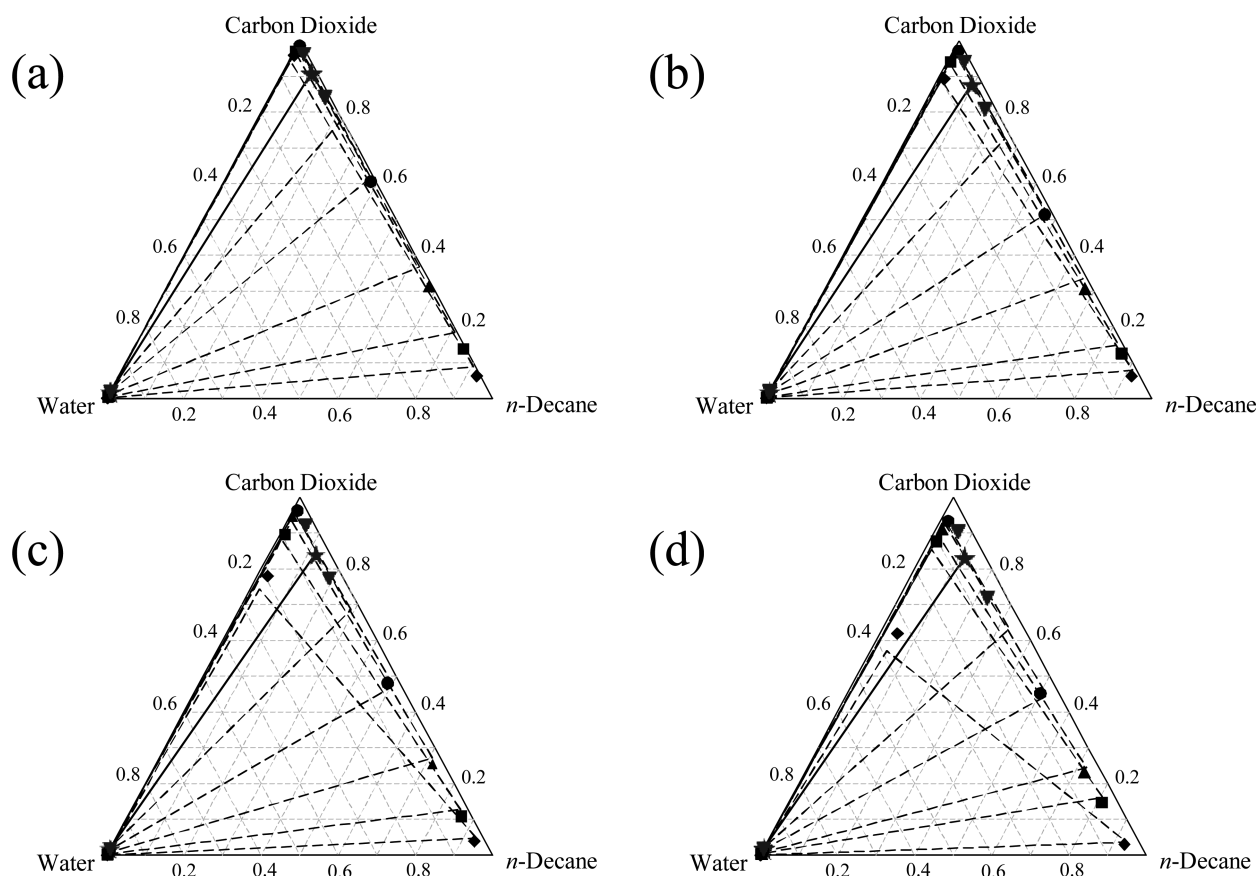


**Figure 6.** Isothermal composition diagram for the (*n*-decane + carbon dioxide + water) system at (a)  $T = 353.11\text{ K}$ , (b)  $T = 373.07\text{ K}$ , (c)  $T = 393.14\text{ K}$ , and (d)  $T = 413.16\text{ K}$ . The symbols represent VLLE data points measured in this work at average pressure: (a)  $\blacklozenge$ ,  $p = 0.94\text{ MPa}$ ;  $\blacksquare$ ,  $p = 2.01\text{ MPa}$ ;  $\blacktriangle$ ,  $p = 4.64\text{ MPa}$ ;  $\bullet$ ,  $p = 9.62\text{ MPa}$ ;  $\blacktriangledown$ ,  $p = 13.32\text{ MPa}$ ; and  $\star$ ,  $p = 13.79\text{ MPa}$ ; (b)  $\blacklozenge$ ,  $p = 1.06\text{ MPa}$ ;  $\blacksquare$ ,  $p = 2.00\text{ MPa}$ ;  $\blacktriangle$ ,  $p = 5.03\text{ MPa}$ ;  $\bullet$ ,  $p = 9.14\text{ MPa}$ ;  $\blacktriangledown$ ,  $p = 15.28\text{ MPa}$ ; and  $\star$ ,  $p = 15.81\text{ MPa}$ ; (c)  $\blacklozenge$ ,  $p = 0.88\text{ MPa}$ ;  $\blacksquare$ ,  $p = 2.08\text{ MPa}$ ;  $\blacktriangle$ ,  $p = 4.72\text{ MPa}$ ;  $\bullet$ ,  $p = 9.59\text{ MPa}$ ;  $\blacktriangledown$ ,  $p = 16.72\text{ MPa}$ ; and  $\star$ ,  $p = 17.30\text{ MPa}$ ; (d)  $\blacklozenge$ ,  $p = 0.95\text{ MPa}$ ;  $\blacksquare$ ,  $p = 3.20\text{ MPa}$ ;  $\blacktriangle$ ,  $p = 4.94\text{ MPa}$ ;  $\bullet$ ,  $p = 10.29\text{ MPa}$ ;  $\blacktriangledown$ ,  $p = 17.08\text{ MPa}$ ; and  $\star$ ,  $p = 18.12\text{ MPa}$ . The continuous line is the measured tie-line between the two coexisting phases remaining after the critical point between the  $\text{CO}_2$ -rich and the decane-rich phases. The discontinuous curves are SAFT-VR predictions of the three-phase equilibrium region for every pressure data point plotted.

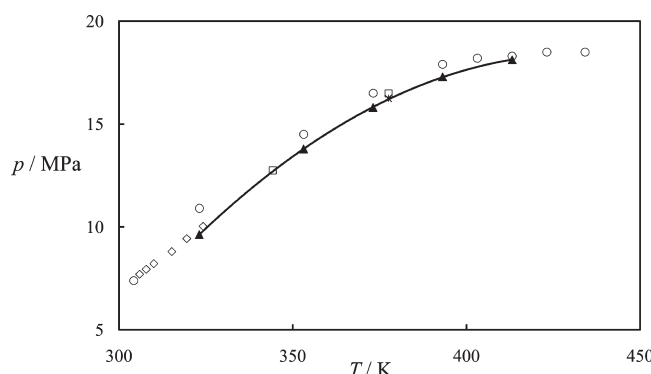


**Figure 7.** Experimental ( $p, T$ ) critical locus. The filled triangles,  $\blacktriangle$ , correspond to the critical states between the  $\text{CO}_2$ -rich and the decane-rich phases in the presence of a third water-rich phase visually observed in this work. The open symbols correspond to critical data points for the binary system (*n*-decane + carbon dioxide):  $\diamond$ , ref 102;  $\circ$ , ref 103;  $*$ , ref 104; and  $\square$ , ref 79. The curve represents a polynomial fit to our data.

with SAFT-VR since at the experimental critical pressure three-phase regions are predicted by the theory. This is a result of the already mentioned overestimation of critical points.<sup>98,94</sup>

## ■ DISCUSSION

As seen in the previous section, mixtures of (*n*-decane + carbon dioxide + water) present a large region of three-phase equilibria. This is a consequence of the type of phase behavior observed for each binary subsystem. Mixtures of (carbon dioxide + water) and (*n*-decane + water) both have a large region of LLE that extends to high temperatures, typical of type III phase behavior in the classification of Scott and van Konynenburg.<sup>20,21</sup> The system (*n*-decane + carbon dioxide) exhibits type II behavior, where the region of LLE is restricted to temperatures below 250 K.<sup>99</sup> The extreme immiscibility of the components of the mixture at the conditions measured results in ternary phase behavior that is relatively close to that of each binary subsystem. The existing literature data for the binaries have been compared with the experimental data of the ternary measured here. In this way, the effect of adding a component on the phase behavior of the other two can be analyzed.

**Influence of Water on the Phase Behavior of (*n*-Decane + Carbon Dioxide).** The experimental data collected for the  $\text{CO}_2$ -rich and the decane-rich phases of the system (*n*-decane + carbon dioxide + water) can be compared to data for the binary system (*n*-decane + carbon dioxide). A comparison at  $T = 373$  and 413 K is shown in Figure 8. The presence of a third water-rich

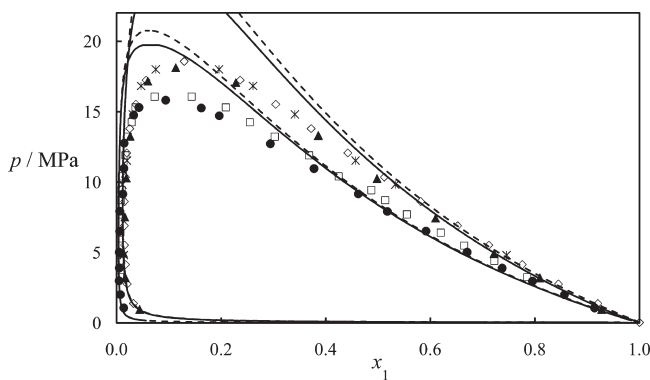


**Figure 8.** Isothermal pressure–composition ( $p, x$ ) phase diagram for the (*n*-decane (1) + carbon dioxide (2) + water (3)) system. The filled symbols represent data gathered during this work for the decane-rich and the carbon-dioxide-rich phases at conditions of three-phase equilibria and temperatures: ●,  $T = 373.07\text{ K}$ ; and ▲,  $T = 413.16\text{ K}$ . The open symbols correspond to measurements for the binary (*n*-decane + carbon dioxide) at the following temperatures: □,  $T = 372.94\text{ K}$ <sup>105</sup> ◇,  $T = 410.93\text{ K}$ <sup>78</sup> and \*,  $T = 411.20\text{ K}$ <sup>106</sup>. The continuous curve corresponds to the SAFT-VR predictions for the decane-rich and the carbon-dioxide-rich phases in the ternary system at conditions of VLLE equilibria and the temperature of our measurements, increasing from bottom to top. The discontinuous curves correspond to the SAFT-VR predictions for the binary system (*n*-decane + carbon dioxide) at the same temperatures.

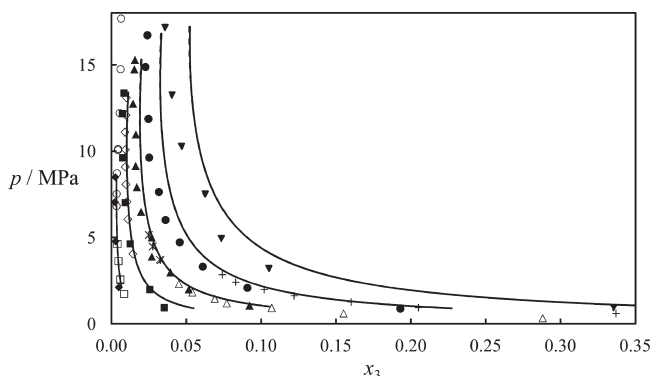


**Figure 9.** Isothermal pressure–composition ( $p, x$ ) phase diagram for the (*n*-decane (1) + carbon dioxide (2) + water (3)) system showing the water content in the  $\text{CO}_2$ -rich phase under VLLE conditions. The filled symbols represent data gathered during this work: ♦,  $T = 323.08\text{ K}$ ; ■,  $T = 353.11\text{ K}$ ; ▲,  $T = 373.07\text{ K}$ ; ●,  $T = 393.14\text{ K}$ ; and ▼,  $T = 413.16\text{ K}$ . The open symbols correspond to published data for the solubility of water in the  $\text{CO}_2$ -rich phase in the binary system (carbon dioxide + water): □,  $T = 323.15\text{ K}$ <sup>107</sup> ○,  $T = 323.15\text{ K}$ <sup>108</sup> ◇,  $T = 353.1\text{ K}$ <sup>109</sup> Δ,  $T = 373.15\text{ K}$ <sup>110</sup> \*,  $T = 373.15\text{ K}$ <sup>107</sup> +,  $T = 393.15\text{ K}$ <sup>110</sup>. The continuous curve corresponds to the SAFT-VR predictions for the  $\text{CO}_2$ -rich phase in the ternary system at conditions of VLLE equilibria and the temperature of our measurements, increasing from left to right. The discontinuous curves (laying underneath) correspond to the SAFT-VR predictions for the binary system (carbon dioxide + water) at the same temperatures.

phase modifies slightly the diagram, and the differences may be noted in the region of highest pressures. The pressure at which *n*-decane and carbon dioxide become miscible for a given composition decreases if water is also present. The theory follows the trend obtained experimentally. The same behavior is observed when we compare the critical locus for the  $\text{CO}_2$ -rich and decane-rich phases with the critical data for (*n*-decane + carbon

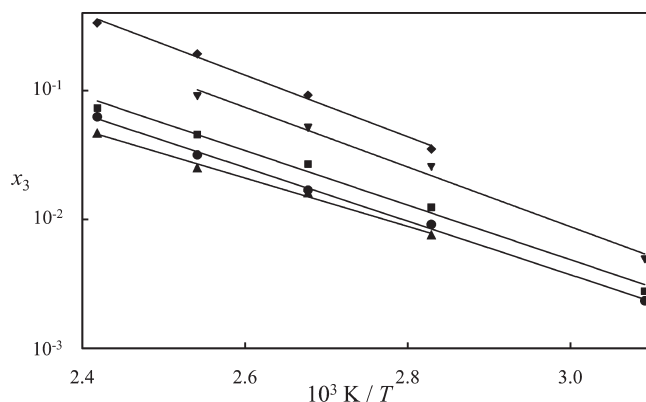


**Figure 10.** Water content in the  $\text{CO}_2$ -rich phase for the system (*n*-decane (1) + carbon dioxide (2) + water (3)) under VLLE conditions as a function of inverse temperature. The filled symbols represent data gathered during this work: ♦,  $p = 0.96 \pm 0.10\text{ MPa}$ ; ▼,  $p = 2.05 \pm 0.06\text{ MPa}$ ; ■,  $p = 4.82 \pm 0.19\text{ MPa}$ ; ●,  $p = 7.43 \pm 0.49\text{ MPa}$ ; ▲,  $p = 9.67 \pm 0.60\text{ MPa}$ . The lines are obtained from a linear fit to each isobar.

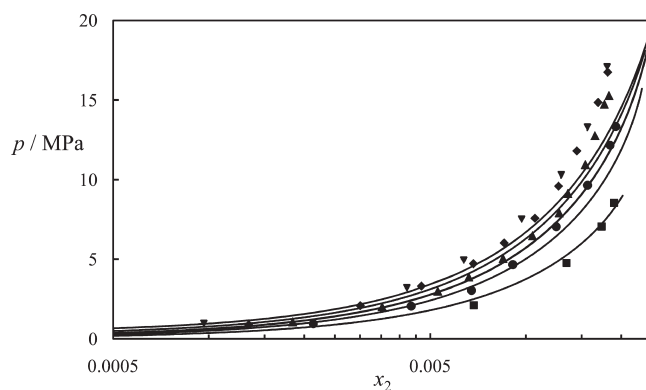


**Figure 11.** Pressure–composition ( $p, x$ ) phase diagram for the (*n*-decane (1) + carbon dioxide (2) + water (3)) system showing the solubility of  $\text{CO}_2$  in the water-rich phase under VLLE conditions for five isotherms. The filled symbols represent data gathered during this work: ■,  $T = 323.08\text{ K}$ ; ●,  $T = 353.11\text{ K}$ ; ▲,  $T = 373.07\text{ K}$ ; ♦,  $T = 393.14\text{ K}$ ; and ▼,  $T = 413.16\text{ K}$ . The continuous curves correspond to the SAFT-VR predictions for the water-rich phase in the ternary system at conditions of VLLE equilibria for the five isotherms, where the temperature increases from bottom to top.

dioxide) published in the literature (see Figure 7). This may be of interest for EOR techniques in which the minimum miscibility pressure (MMP) is a design parameter for miscible flooding processes. The conclusion from this analysis is that water acts as a weak cosolvent at high pressure.

**Influence of *n*-Decane on the Phase Behavior of (Carbon Dioxide + Water).** Similarly, we study the effect of *n*-decane on the phase behavior of (carbon dioxide + water) comparing our experimental data to available binary data. We address here the study of the  $\text{CO}_2$ -rich and the water-rich phases separately. A comparison of the water content of the  $\text{CO}_2$  phase for the ternary system with that for the binary is shown in Figure 9. The solubilities for the ternary system overlap with those for the binary to within experimental uncertainty. The predictions of the theory are consistent with experiment: Those for the binary are not shown here as a different curve because they lay over those for the ternaries, and only a very small increase in solubility

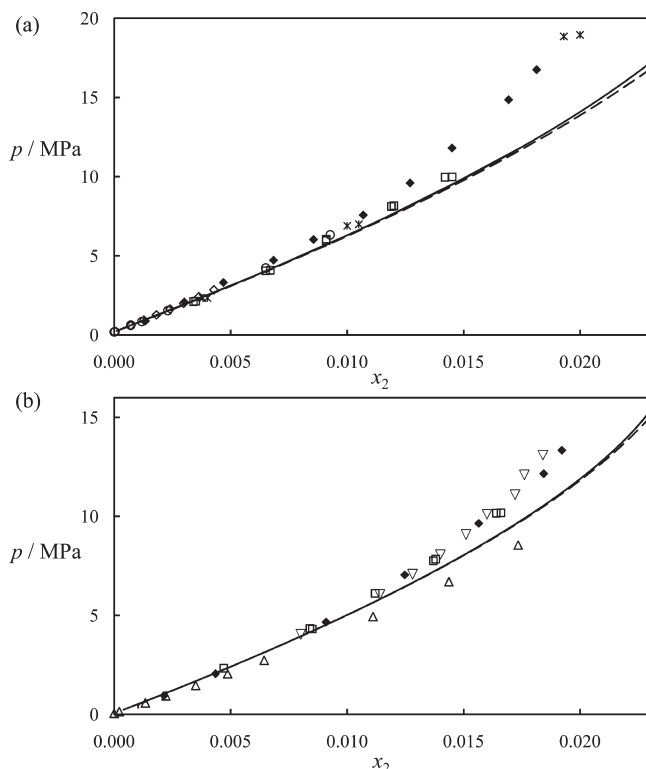


**Figure 12.** Isothermal pressure–composition ( $p, x$ ) phase diagram for the (*n*-decane (1) + carbon dioxide (2) + water (3)) system showing the solubility of  $\text{CO}_2$  in the water-rich phase under VLLE conditions. The filled diamonds,  $\blacklozenge$ , represent data gathered during this work at (a)  $T = 393.14 \text{ K}$  and (b)  $T = 353.11 \text{ K}$ . The open symbols correspond to published data for the solubility of  $\text{CO}_2$  in the water-rich phase for the binary (carbon dioxide + water): (a)  $\circ$ ,  $T = 393.17 \text{ K}$ ;<sup>111</sup>  $\diamond$ ,  $T = 393.15 \text{ K}$ ;<sup>110\*</sup>  $\square$ ,  $T = 393.15 \text{ K}$ ;<sup>112</sup> and  $\square$ ,  $T = 393.19 \text{ K}$ ;<sup>113</sup> (b)  $\Delta$ ,  $T = 353.11 \text{ K}$ ;<sup>111</sup>  $\square$ ,  $T = 353.5 \text{ K}$ ;<sup>113</sup> and  $\nabla$ ,  $T = 353.1 \text{ K}$ .<sup>109</sup> The continuous curve corresponds to the SAFT-VR predictions for the water-rich phase in the ternary system at conditions of VLLE equilibria. The discontinuous curve corresponds to the SAFT-VR predictions for the water-rich phase in the (carbon dioxide + water) binary system.

can be seen at the highest pressures of study. The measurements of water in the gas phase can also be tested as in previous work<sup>100</sup> to check whether adsorption of water in the transfer lines to the gas chromatograph may have occurred. The solubilities of water in the gas phase are plotted versus the inverse of temperature in Figure 10 for selected pressures. Note that our experimental data are not precisely isobaric, but we are plotting data taken at relatively close pressures. For low compositions of water in the gas phase the dependency of composition is assumed to be based on the vapor pressure of water so that for a given pressure a linear behavior is seen in this kind of plot. As seen in the figure, also different isobars exhibit parallel trends. Because this linearity is followed, adsorption of water may be considered negligible.

The solubilities of  $\text{CO}_2$  in the water-rich phase are plotted in Figure 11 for the five isotherms measured and compared to the predictions with SAFT-VR. In general there is a reasonable level of agreement, although deviations increase with increase in pressure. These solubilities obtained for the ternary system at conditions of three phase equilibria agree well with the literature data for the binary system, as is shown in Figure 12a for the

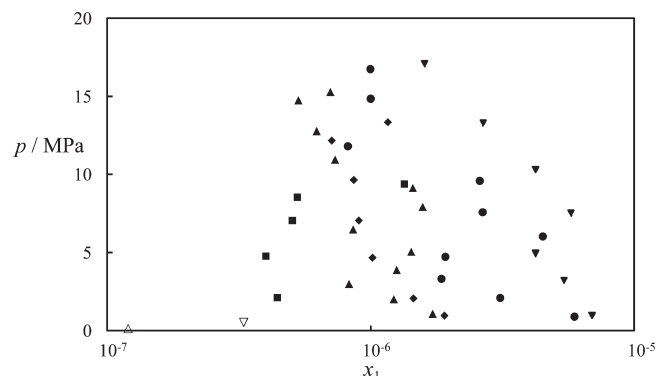
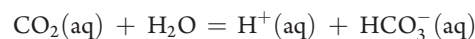


**Figure 13.** Isothermal pressure–composition ( $p, x$ ) phase diagram for the (*n*-decane (1) + carbon dioxide (2) + water (3)) system showing the *n*-decane content in the water-rich phase under VLLE conditions. The filled symbols represent data gathered during this work:  $\blacksquare$ ,  $T = 323.08 \text{ K}$ ;  $\blacklozenge$ ,  $T = 353.11 \text{ K}$ ;  $\blacktriangle$ ,  $T = 373.07 \text{ K}$ ;  $\bullet$ ,  $T = 393.14 \text{ K}$ ; and  $\nabla$ ,  $T = 413.16 \text{ K}$ . The open symbols correspond to published data for the solubility of *n*-decane in the water-rich phase in the binary (*n*-decane + water) at  $\Delta$ ,  $T = 373.15 \text{ K}$ ,<sup>59</sup> and  $\nabla$ ,  $T = 424.65 \text{ K}$ .<sup>59</sup>

isotherm at  $T = 393.14 \text{ K}$ . Such close agreement was expected due to the low solubility of the third component, *n*-decane, in the water phase. This is also shown by the theory: in the same figure, the predictions for the binary and the ternary system are compared. Small deviations only appear at the highest pressures. Better agreement with the theory can be seen at lower temperatures as shown in Figure 12 b for  $T = 353.11 \text{ K}$ , although at this temperature there is a greater scatter between different literature sources. Concluding the analysis of the effect of *n*-decane on the phase behavior of (carbon dioxide + water), it has been shown that the phase equilibrium is practically unaltered when *n*-decane is also present and only minor differences are seen at the highest pressures of study.

It is known that the dissolution of carbon dioxide in water takes place not only by physical equilibrium but also chemically according to the following reaction



neglecting the second dissociation to carbonate, which is only important at high pH. The fraction of carbon dioxide dissociated in the aqueous phase is however negligible compared with experimental error. An estimation can be made using the first constant of dissociation, which varies with temperature as<sup>101</sup>

$$\log_{10} K^\ominus = -3404.71 (\text{K}/\text{T}) + 14.8435 - 0.032786 (\text{T}/\text{K}) \quad (7)$$

Neglecting nonideality (i.e., setting the activity coefficients to unity), the fraction  $\alpha$  of  $\text{CO}_2$  molecules dissociated in the liquid phase is given approximately by

$$\alpha \approx \sqrt{m^\ominus K^\ominus / m_{\text{CO}_2}} \quad (8)$$

where  $m^\ominus = 1 \text{ mol kg}^{-1}$  is the standard molality. For example, at  $T = 413 \text{ K}$  and  $p = 1 \text{ MPa}$ ,  $K = 1.1 \times 10^{-7}$  and  $m_{\text{CO}_2} \approx 0.06 \text{ mol kg}^{-1}$  so that  $\alpha \approx 1.4 \times 10^{-3}$ . The fraction dissociated is in any case between  $3 \times 10^{-4}$  and  $3 \times 10^{-3}$  at all temperatures and pressures in the range of study. No further consideration was given to chemical equilibria in the aqueous phase.

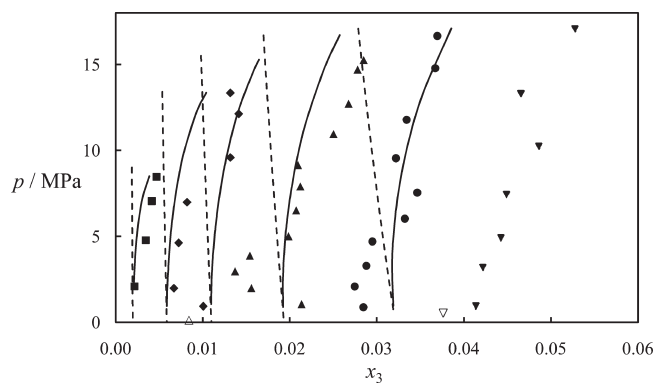


**Figure 14.** Isothermal pressure–composition ( $p, x$ ) phase diagram for the (*n*-decane (1) + carbon dioxide (2) + water (3)) system showing the water content in the decane-rich liquid phase under VLLE conditions. The filled symbols represent data gathered during this work: ■,  $T = 323.08\text{ K}$ ; ◆,  $T = 353.11\text{ K}$ ; ▲,  $T = 373.07\text{ K}$ ; ●,  $T = 393.14\text{ K}$ ; and ▽,  $T = 413.16\text{ K}$ . The open symbols correspond to published data for the solubility of water in the decane-rich phase in the binary (*n*-decane + water) at  $\Delta$ ,  $T = 374.15\text{ K}^{59}$  and  $\nabla$ ,  $T = 424.65\text{ K}^{59}$ . The continuous curves correspond to the SAFT-VR predictions for the decane-rich phase in the ternary system at conditions of VLLE equilibria at the same temperatures, increasing from left to right. The discontinuous curves correspond to the SAFT-VR predictions of the decane-rich phase in the (*n*-decane + water) binary system.

**Influence of Carbon Dioxide on the Phase Behavior of (*n*-Decane + Water).** Next, we study the effect of carbon dioxide on the phase behavior of (*n*-decane + water). Again we refer first to the water-rich phase and then to the decane-rich phase. The measured mole fractions of *n*-decane in the water-rich phase are of the order of ppm as recorded in Table 3. Although they present some scatter (see Figure 13), the order of magnitude may be approximately 10 times higher than that reported for the solubility of *n*-decane in pure water at  $T = 374.15\text{ K}$  and  $T = 424.65\text{ K}$  and low pressure.<sup>59</sup> Our predictions with SAFT-VR and the chosen binary parameter to model the interactions between water and *n*-decane underestimate considerably the solubility of *n*-decane in the water phase (e.g.,  $2.2 \times 10^{-15}$  at  $T = 373.1\text{ K}$  and  $p = 15\text{ MPa}$ ) as shown in Table 3, but the predicted compositions are slightly higher than for the binary ( $1.6 \times 10^{-15}$  at the same temperature and pressure). This effect could be corrected using a different  $k_{ij}$  value for this phase, but this was out of the scope of this work.

The measurements of water in the decane-rich phase are plotted in Figure 14. In general experimental values for the ternary system show a higher water concentration than that for the binary (*n*-decane + water).<sup>59</sup> However, experimental data for this binary system at the conditions of the present study are scarce. The SAFT-VR EOS also predicts higher solubilities of water in *n*-decane when the third component is present, although this effect is more noticeable at higher pressures; in fact, the solubility of water in *n*-decane for the binary system decreases with pressure, whereas it is enhanced with pressure in the case of the ternary. Experimentally, it is difficult to avoid completely contamination of the decane-rich phase with the water-rich phase, and larger water peaks may randomly be measured during the sampling procedure. These peaks were however discarded during the analysis. Finally, regarding the effect of carbon dioxide on the mutual solubility of (*n*-decane + water), we may conclude that it acts as a mild cosolvent. This effect of cosolvency is consistent with the reduction of interfacial tension that is observed between the two

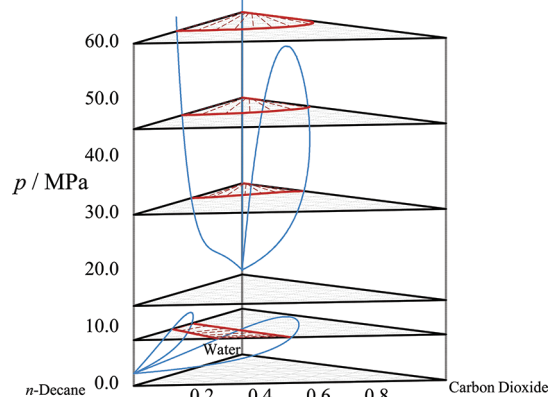


**Figure 15.** Isothermal pressure–composition ( $p, x$ ) prismatic diagram for the (*n*-decane + carbon dioxide + water) system at a reduced temperature of 0.95 times the calculated critical temperature for *n*-decane ( $T = 582.2\text{ K}$  calculated with the experimental critical temperature for *n*-decane) calculated with SAFT-VR. Regions of two-phase equilibria appear delimited by continuous red thick curves with some tie-lines traced with thin dashed red lines. The two phase coexisting regions for the binary subsystems appear in the lateral sides of the prismatic diagram delimited by continuous blue lines. The remaining are homogeneous one-phase regions.

saturated phases of (*n*-decane + water) with additions of carbon dioxide to the system.<sup>8</sup>

Having a global theory is advantageous to extend the study to temperatures beyond the limits of our experimental technique. For example, Figure 15 shows an isotherm at a reduced temperature 0.95 times the calculated critical temperature for *n*-decane (or  $T = 582\text{ K}$  considering the experimental critical temperature for this component). At this higher temperature a markedly different behavior is observed. Whereas, at low temperature, the phase diagram was dominated by regions of three-phase equilibria, here VLE regions and critical states are the main features. The temperature chosen lies below the critical temperature of both water (647 K) and *n*-decane (617 K), but the critical line for the mixture (carbon dioxide + water) and one of the two critical lines present in (*n*-decane + water) are crossed. This is observed in the diagram by means of the closed envelopes; these are VLE regions which finish at the critical pressure of each binary mixture at the temperature of study. As is common at lower temperatures there is also a critical pressure for (*n*-decane + carbon dioxide) at this temperature. In the case of the binary (*n*-decane + water) when the vapor pressure of water is exceeded an LLE region appears and extends to higher pressures (open envelope). But below that pressure and above the vapor pressure for *n*-decane it is interesting to note that areas at which the three components are miscible in every proportion can be distinguished. This could be of interest for processes where the three components, water, CO<sub>2</sub> and *n*-decane, were required to form a unique phase.

## CONCLUSIONS

We have developed a new experimental apparatus for measuring phase equilibria at reservoir conditions. In the design of this analytical apparatus, special care was taken to ensure that the sampling system was reliable. Our approach to this problem involved the incorporation of a magnetic

recirculating pump that yields good reproducibility of the analysis of liquid samples.

The apparatus has been validated against literature data for the system (*n*-decane + carbon dioxide) at temperatures of  $T = 311.02$  K and  $T = 344.31$  K. New data for the system (*n*-decane + carbon dioxide + water) has been gathered at conditions of three-phase equilibria. Five isotherms from  $T = 323.08$ – $413.16$  K and pressures from  $\sim 0.9$  MPa up to the critical pressure between the carbon-dioxide-rich and the decane-rich phases which is at  $9.38$ – $18.12$  MPa have been measured for this system. The analysis of the system has been complemented with calculations performed with SAFT-VR using three temperature-independent binary interaction parameters. An extension of the Hudson and McCoubrey combining rules was used to calculate one of these parameters, while the others were obtained by fitting to data for the binary system.

We have compared the experimental VLLE data for the ternary system (*n*-decane + carbon dioxide + water) with literature data for the corresponding binary subsystems and carried out comparisons of the phase equilibria predicted with SAFT-VR. Overall, the comparison between the mutual solubilities of the three components at conditions of three-phase equilibria for the ternary system and the solubility of the components in the corresponding binary subsystems shows small differences. The solubility of water in *n*-decane and that of *n*-decane in water seem to increase slightly with respect to the binary (*n*-decane + water) when CO<sub>2</sub> is present, at the same conditions. The solubility of carbon dioxide in water decreases slightly in the presence of *n*-decane at the highest pressures of study and that of water in carbon dioxide shows no appreciable change, if we compare to the binary system (carbon dioxide + water), although the theory predicts a very small increase. A similar comparison with the binary (*n*-decane + carbon dioxide) system shows that, while the content of *n*-decane in the carbon dioxide phase is not affected, that of the carbon dioxide in the *n*-decane phase increases when water is added. As a result, the solubility of the carbon dioxide in the decane-rich phase increases but that for the water-rich phase decreases. In general these effects are small at low pressure but more significant as pressure increases.

## AUTHOR INFORMATION

### Corresponding Author

\*E-mail: m.trusler@imperial.ac.uk.

## ACKNOWLEDGMENT

The authors gratefully acknowledge the financial support of Shell International Exploration and Production B.V. in sponsoring this project and further support from EPSRC (Grant EP/E016340/1) to the Molecular Systems Engineering group.

## REFERENCES

- (1) Kane, A. V. *J. Pet. Technol.* **1979**, *31*, 217–231.
- (2) Langston, M. V.; Hoadley, S. F.; Young, D. N. Definitive CO<sub>2</sub> Flooding Response in the SACROC Unit. SPE Enhanced Oil Recovery Symposium, 16–21 April 1988, Tulsa, Oklahoma.
- (3) Blunt, M.; Fayers, F. J.; Orr, F. M., Jr. *Energy Convers. and Mgmt.* **1993**, *34*, 1197–1204 (Proceedings of the International Energy Agency Carbon Dioxide Disposal Symposium).
- (4) Orr, F. M. *J. Pet. Technol.* **2004**, *56*, 90–97.
- (5) Malik, Q. M.; Islam, M. R. CO<sub>2</sub> Injection in the Weyburn Field of Canada: Optimization of Enhanced Oil Recovery and Greenhouse Gas Storage with Horizontal Wells. SPE/DOE Improved Oil Recovery Symposium, 3–5 April 2000, Tulsa, Oklahoma.
- (6) Moberg, R.; Stewart, D. B.; Stachniak, D. The IEA Weyburn CO<sub>2</sub> Monitoring and Storage Project. In *Greenhouse Gas Control Technologies—6th International Conference*; Gale, J., Kaya, Y., Eds.; Pergamon: Oxford, 2003; pp 219–224.
- (7) Preston, C.; Monea, M.; Jazrawi, W.; Brown, K.; Whittaker, S.; White, D.; Law, D.; Chalaturnyk, R.; Rostro, B. *Fuel Process. Technol.* **2005**, *86*, 1547–1568.
- (8) Georgiadis, A.; Maitland, G.; Trusler, J. P. M.; Bismarck, A. *J. Chem. Eng. Data*, in press; DOI: 10.1021/je200825j.
- (9) Ciotta, F.; Maitland, G.; Smietana, M.; Trusler, J. P. M.; Vesovic, V. *J. Chem. Eng. Data* **2009**, *54*, 2436–2443.
- (10) Qin, J.; Rosenbauer, R. J.; Duan, Z. *J. Chem. Eng. Data* **2008**, *53*, 1246–1249.
- (11) Jarne, C.; Blanco, S. T.; Gallardo, M. A.; Rauzy, E.; Otín, S.; Velasco, I. *Energy Fuels* **2004**, *18*, 396–404.
- (12) Dhima, A.; de Hemptinne, J.-C.; Jose, J. *Ind. Eng. Chem. Res.* **1999**, *38*, 3144–3161.
- (13) Song, K. Y.; Holder, G. D.; Warzinski, R. P. *Ind. Eng. Chem. Res.* **2008**, *47*, 459–469.
- (14) Beltrán, J. G.; Servio, P. *J. Chem. Eng. Data* **2008**, *53*, 1745–1749.
- (15) Seo, Y.-T.; Lee, H.; Yoon, J.-H. *J. Chem. Eng. Data* **2001**, *46*, 381–384.
- (16) Gil, L.; Avila, S.; García-Giménez, P.; Blanco, S. T.; Berro, C.; Otín, S.; Velasco, I. *Ind. Eng. Chem. Res.* **2006**, *45*, 3974–3980.
- (17) Brunner, G.; Teich, J.; Dohrn, R. *Fluid Phase Equilib.* **1994**, *100*, 253–268.
- (18) Okafor, M. N. Ph.D. Thesis. University of Missouri, Rolla, MO, 1987.
- (19) Scott, R. L.; van Konynenburg, P. H. *Discuss. Faraday Soc.* **1970**, *49*, 87–97.
- (20) van Konynenburg, P. H.; Scott, R. L. *Philos. Trans. R. Soc. London* **1980**, *298*, 495–540.
- (21) Diamond, L. W.; Akinfiev, N. N. *Fluid Phase Equilib.* **2003**, *208*, 265–290.
- (22) Spycher, N.; Pruess, K.; Ennis-King, J. *Geochim. Cosmochim. Acta* **2003**, *67*, 3015–3031.
- (23) Shaw, D. G.; Maczynski, A.; Goral, M.; Wisniewska-Gocłowska, B.; Skrzecz, A.; Owczarek, I.; Blazej, K.; Haulait-Pirson, M.-C.; Hefter, G. T.; Kapuku, F.; Maczynska, Z.; Szafranski, A. *J. Phys. Chem. Ref. Data* **2006**, *35*, 93–151.
- (24) Peng, D.-Y.; Robinson, D. B. *Ind. Eng. Chem. Fundam.* **1976**, *15*, 59–64.
- (25) Soave, G. *Chem. Eng. Sci.* **1972**, *27*, 1197–1203.
- (26) van der Waals, J. D. Ph.D. Thesis, Leyden, 1873. In *On the Continuity of the Gaseous and Liquid States*; Rowlinson, J. S., Ed.; Dover Phoenix Editions: Mineola, NY, 2004.
- (27) Kontogeorgis, G. M.; Voutsas, E. C.; Yakoumis, I. V.; Tassios, D. P. *Ind. Eng. Chem. Res.* **1996**, *35*, 4310–4318.
- (28) Wertheim, M. S. *J. Stat. Phys.* **1984**, *35*, 19.
- (29) Wertheim, M. S. *J. Stat. Phys.* **1984**, *35*, 35.
- (30) Wertheim, M. S. *J. Stat. Phys.* **1986**, *42*, 459.
- (31) Wertheim, M. S. *J. Stat. Phys.* **1986**, *42*, 477.
- (32) Chapman, W. G.; Gubbins, K. E.; Jackson, G.; Radosz, M. *Fluid Phase Equilib.* **1989**, *52*, 31–38.
- (33) Chapman, W. G.; Gubbins, K. E.; Jackson, G.; Radosz, M. *Ind. Eng. Chem. Res.* **1990**, *29*, 1709–1721.
- (34) Wertheim, M. S. *J. Chem. Phys.* **1986**, *85*, 2929–2936.
- (35) Wertheim, M. S. *J. Chem. Phys.* **1987**, *87*, 7323–7331.
- (36) Gil-Villegas, A.; Galindo, A.; Whitehead, P. J.; Mills, S. J.; Jackson, G.; Burgess, A. N. *J. Chem. Phys.* **1997**, *106*, 4168–4186.
- (37) Galindo, A.; Davies, L. A.; Gil-Villegas, A.; Jackson, G. *Mol. Phys.* **1998**, *93*, 241–252.
- (38) Blas, F. J.; Vega, L. F. *Mol. Phys.* **1997**, *92*, 135–150.

- (40) Gross, J.; Sadowski, G. *Fluid Phase Equilib.* **2000**, *168*, 183–199.  
 (41) Gross, J.; Sadowski, G. *Ind. Eng. Chem. Res.* **2001**, *40*, 1244–1260.  
 (42) Müller, E. A.; Gubbins, K. E. Associating Fluids and Fluid Mixtures. In *Equations of State for Fluids and Fluid Mixtures*; Sengers, J. V., Kayser, R. F., Peters, C. J., White, H. J., Eds.; Elsevier: Amsterdam, 2000; Chapter 12.  
 (43) Müller, E. A.; Gubbins, K. E. *Ind. Eng. Chem. Res.* **2001**, *40*, 2193–2211.  
 (44) Economou, I. G. *Ind. Eng. Chem. Res.* **2002**, *41*, 953–962.  
 (45) Tan, S. P.; Adidharma, H.; Radosz, M. *Ind. Eng. Chem. Res.* **2008**, *47*, 8063–8082.  
 (46) McCabe, C.; Galindo, A. SAFT Associating Fluids and Fluids Mixtures. In *Applied Thermodynamics of Fluids*; Goodwin, A. R. H., Sengers, J. V., Eds.; Royal Society of Chemistry: London, 2010; Chapter 8.  
 (47) Galindo, A.; Whitehead, P. J.; Jackson, G.; Burgess, A. N. *J. Phys. Chem.* **1996**, *100*, 6781–6792.  
 (48) Yakoumis, I. V.; Kontogeorgis, G. M.; Voutsas, E. C.; Hendriks, E. M.; Tassios, D. P. *Ind. Eng. Chem. Res.* **1998**, *37*, 4175–4182.  
 (49) Voutsas, E. C.; Boulogouris, G. C.; Economou, I. G.; Tassios, D. P. *Ind. Eng. Chem. Res.* **2000**, *39*, 797–804.  
 (50) Li, X.-S.; Englezos, P. *Fluid Phase Equilib.* **2004**, *224*, 111–118.  
 (51) Karakatsani, E. K.; Kontogeorgis, G. M.; Economou, I. G. *Ind. Eng. Chem. Res.* **2006**, *45*, 6063–6074.  
 (52) Oliveira, M. B.; Coutinho, J. A. P.; Queimada, A. J. *Fluid Phase Equilib.* **2007**, *258*, 58–66.  
 (53) Aparicio-Martínez, S.; Hall, K. R. *Fluid Phase Equilib.* **2007**, *254*, 112–125.  
 (54) Nguyen-Huynh, D.; de Hemptinne, J.-C.; Lugo, R.; Passarello, J.-P.; Tobaly, P. *Ind. Eng. Chem. Res.* **2011**, *50*, 7467–7483.  
 (55) Emborsky, C. P.; Cox, K. R.; Chapman, W. G. *Ind. Eng. Chem. Res.* **2011**, *50*, 7791–7799.  
 (56) Papaioannou, V.; Adjiman, C. S.; Jackson, G.; Galindo, A. *Fluid Phase Equilib.* **2011**, *306*, 82–96.  
 (57) Hudson, G. H.; McCoubrey, J. C. *Trans. Faraday Soc.* **1960**, *56*, 761–766.  
 (58) Haslam, A. J.; Galindo, A.; Jackson, G. *Fluid Phase Equilib.* **2008**, *266*, 105–128.  
 (59) Economou, I. G.; Heidman, J. L.; Tsionopoulos, C.; Wilson, G. M. *AIChE J.* **1997**, *43*, 535–546.  
 (60) Tsionopoulos, C. *Fluid Phase Equilib.* **1999**, *156*, 21–33.  
 (61) Patel, B. H.; Paricaud, P.; Galindo, A.; Maitland, G. C. *Ind. Eng. Chem. Res.* **2003**, *42*, 3809–3823.  
 (62) Vega, L. F.; Llorell, F.; Blas, F. J. *J. Phys. Chem. B* **2009**, *113*, 7621–7630.  
 (63) Kontogeorgis, G. M.; Michelsen, M. L.; Folas, G. K.; Derawi, S.; von Solms, N.; Stenby, E. H. *Ind. Eng. Chem. Res.* **2006**, *45*, 4869–4878.  
 (64) Kontogeorgis, G. M.; Folas, G. K.; Muro-Suñé, N.; Roca Leon, F.; Michelsen, M. L. *Oil Gas Sci. Technol. - Rev. IFP* **2008**, *63*, 305–319.  
 (65) Kontogeorgis, G. M.; Tsivintzelis, I.; Michelsen, M. L.; Stenby, E. H. *Fluid Phase Equilib.* **2011**, *301*, 244–256.  
 (66) Valtz, A.; Chapoy, A.; Coquelet, C.; Paricaud, P.; Richon, D. *Fluid Phase Equilib.* **2004**, *226*, 333–344.  
 (67) dos Ramos, M. C.; Blas, F. J.; Galindo, A. *Fluid Phase Equilib.* **2007**, *261*, 359–365.  
 (68) dos Ramos, M. C.; Blas, F. J.; Galindo, A. *J. Phys. Chem. C* **2007**, *111*, 15924–15934.  
 (69) Mac Dowell, N.; Llorell, F.; Adjiman, C. S.; Jackson, G.; Galindo, A. *Ind. Eng. Chem. Res.* **2010**, *49*, 1883–1899.  
 (70) Gross, J. *AIChE J.* **2005**, *51*, 2556–2568.  
 (71) Llorell, F.; Vega, L. F. *J. Phys. Chem. B* **2006**, *110*, 1350–1362.  
 (72) Blas, F. J.; Galindo, A. *Fluid Phase Equilib.* **2002**, *194*–197, 501–509.  
 (73) Galindo, A.; Blas, F. J. *J. Phys. Chem. B* **2002**, *106*, 4503–4515.  
 (74) Míguez, J. M.; dos Ramos, M. C.; Piñeiro, M. M.; Blas, F. J. *J. Phys. Chem. B* **2011**, *115*, 9604–9617.  
 (75) Ruffine, L.; Trusler, J. P. M. *J. Chem. Thermodyn.* **2010**, *42*, 605–611.  
 (76) Peletier, F.; Trusler, J. P. M.; Goodwin, A. R. H.; Maitland, G. C. *Rev. Sci. Instrum.* **2005**, *76*, 105103.  
 (77) Lemmon, E. W.; McLinden, M. O.; Friend, D. G. Thermo-physical Properties of Fluid Systems. In *NIST Chemistry WebBook, NIST Standard Reference Database Number 69*; Linstrom, P. J., Mallard, W. G., Eds.; **2011**. <http://webbook.nist.gov>.  
 (78) Reamer, H. H.; Sage, B. H. *J. Chem. Eng. Data* **1963**, *8*, 508–513.  
 (79) Nagarajan, N.; Robinson, R. L. *J. Chem. Eng. Data* **1986**, *31*, 168–171.  
 (80) Chou, G. F.; Forbert, R. R.; Prausnitz, J. M. *J. Chem. Eng. Data* **1990**, *35*, 26–29.  
 (81) Han, B.; Peng, D. Y.; Fu, C. T.; Vilcsak, G. *Can. J. Chem. Eng.* **1992**, *270*, 1164–1171.  
 (82) Iwai, Y.; Hosotani, N.; Morotomi, T.; Koga, Y.; Arai, Y. *J. Chem. Eng. Data* **1994**, *39*, 900–902.  
 (83) Jennings, D. W.; Schucker, R. C. *J. Chem. Eng. Data* **1996**, *41*, 831–838.  
 (84) Shaver, R. D.; Robinson, R. L.; Gasem, K. A. M. *Fluid Phase Equilib.* **2001**, *179*, 43–66.  
 (85) Taylor, B. N.; Kuyatt, C. E. *Guidelines for Evaluating and Expressing the Uncertainty of NIST Measurement Results*; NIST Technical Note 1297; NIST: Gaithersburg, MD, 1993.  
 (86) Paricaud, P.; Galindo, A.; Jackson, G. *Ind. Eng. Chem. Res.* **2004**, *43*, 6871–6889.  
 (87) Clark, G. N. I.; Haslam, A. J.; Galindo, A.; Jackson, G. *Mol. Phys.* **2006**, *104*, 3561–3581.  
 (88) Lide, D. R. *CRC Handbook of Chemistry and Physics*, 86th ed.; CRC Press/Taylor and Francis: Boca Raton, FL, 2005.  
 (89) Buckingham, A. D. Electric moments of molecules. In *Physical Chemistry: An Advanced Treatise, Vol. 4, Molecular Properties*; Eyring, H., Henderson, D., Jost, W., Eds.; Academic Press: New York/London, 1970; Chapter 8.  
 (90) Namiot, A. Y.; Skripka, V. G.; Lotter, Y. G. *Deposited Doc. VINITI 1976*, *1*–13. (as cited in Detherm)  
 (91) Sultanov, R. G.; Skripka, V. G. *Deposited Doc. VINITI 1972*, *12*. (as cited in Detherm)  
 (92) Pereira, F. E.; Jackson, G.; Galindo, A.; Adjiman, C. S. *Fluid Phase Equilib.* **2010**, *299*, 1–23.  
 (93) Pereira, F. E.; Jackson, G.; Galindo, A.; Adjiman, C. S. *Comput. Chem. Eng.* **2011**, DOI: 10.1016/j.compchemeng.2011.07.009.  
 (94) Forte, E.; Llorell, F.; Vega, L. F.; Trusler, J. P. M.; Galindo, A. *J. Chem. Phys.* **2011**, *134*, 154102.  
 (95) McCabe, C.; Kiselev, S. B. *Fluid Phase Equilib.* **2004**, *219*, 3–9.  
 (96) McCabe, C.; Kiselev, S. B. *Ind. Eng. Chem. Res.* **2004**, *43*, 2839–2851.  
 (97) Sun, L.; Zhao, H.; Kiselev, S. B.; McCabe, C. *J. Phys. Chem. B* **2005**, *109*, 9047–9058.  
 (98) Sengers, J. M. H. L. *Fluid Phase Equilib.* **1999**, *158*–160, 3–17.  
 (99) Kulkarni, A. A.; Zarath, B. Y.; Luks, K. D.; Kohn, J. P. *J. Chem. Eng. Data* **1974**, *19*, 92–94.  
 (100) Chapoy, A.; Coquelet, C.; Richon, D. *Fluid Phase Equilib.* **2005**, *230*, 210–214.  
 (101) Harned, H. S.; Davis, R. *J. Am. Chem. Soc.* **1943**, *65*, 2030–2037.  
 (102) Gurdial, G. S.; Foster, N. R.; Yun, S. L. J.; Tilly, K. D. *ACS Symp. Ser.* **1993**, *514*, 34–45.  
 (103) Chester, T. L.; Haynes, B. S. *J. Supercrit. Fluids* **1997**, *11*, 15–20.  
 (104) Polikronidi, N.; Batyrova, R.; Abdulagatov, I.; Stepanov, G. *Int. J. Thermophys.* **2006**, *27*, 729–759.  
 (105) Jimenez-Gallegos, R.; Galicia-Luna, L. A.; Elizalde-Solis, O. *J. Chem. Eng. Data* **2006**, *51*, 1624–1628.  
 (106) Inomata, H.; Tuchiya, K.; Arai, K.; Saito, S. *J. Chem. Eng. Jpn.* **1986**, *19*, 386–391.  
 (107) Coan, C. R.; King, A. D. *J. Am. Chem. Soc.* **1971**, *93*, 1857–1862.  
 (108) Briones, J. A.; Mullins, J. C.; Thies, M. C.; Kim, B. U. *Fluid Phase Equilib.* **1987**, *36*, 235–246.

- (109) Bamberger, A.; Sieder, G.; Maurer, G. *J. Supercrit. Fluids* **2000**, *17*, 97–110.
- (110) Mueller, G. Ph.D. Thesis. University of Kaiserslautern, 1983.
- (111) Kiepe, J.; Horstmann, S.; Fischer, K.; Gmehling, J. *Ind. Eng. Chem. Res.* **2002**, *41*, 4393–4398.
- (112) Prutton, C. F.; Savage, R. L. *J. Am. Chem. Soc.* **1945**, *67*, 1550–1554.
- (113) Nighswander, J. A.; Kalogerakis, N.; Mehrotra, A. K. *J. Chem. Eng. Data* **1989**, *34*, 355–360.